

Cosmological Tests of Gravity

Bhuvnesh Jain & Justin Khoury

*Center for Particle Cosmology, Department of Physics and Astronomy,
University of Pennsylvania, Philadelphia, PA 19104*

Abstract

Modifications of general relativity provide an alternative explanation to dark energy for the observed acceleration of the universe. We review recent developments in modified gravity theories, focusing on higher dimensional approaches and chameleon/ $f(R)$ theories. We classify these models in terms of the screening mechanisms that enable such theories to approach general relativity on small scales (and thus satisfy solar system constraints). We describe general features of the modified Friedman equation in such theories.

The second half of this review describes experimental tests of gravity in light of the new theoretical approaches. We summarize the high precision tests of gravity on laboratory and solar system scales. We describe in some detail tests on astrophysical scales ranging from \sim kpc (galaxy scales) to \sim Gpc (large-scale structure). These tests rely on the growth and inter-relationship of perturbations in the metric potentials, density and velocity fields which can be measured using gravitational lensing, galaxy cluster abundances, galaxy clustering and the Integrated Sachs-Wolfe effect. A robust way to interpret observations is by constraining effective parameters, such as the ratio of the two metric potentials. Currently tests of gravity on astrophysical scales are in the early stages — we summarize these tests and discuss the interesting prospects for new tests in the coming decade.

Keywords: Modified Gravity, Cosmology

Contents

1	Introduction	2
1.1	Approaches to Modify Gravity	3
1.2	Newtonian Tests	5
1.3	Post-Newtonian Tests	6

Email address: bjain@physics.upenn.edu, jkhoury@physics.upenn.edu (Bhuvnesh Jain & Justin Khoury)

2	Modified Gravity Theories	7
2.1	Chameleon/ $f(R)$ Field Theories	7
2.1.1	Thin-Shell Screening	10
2.1.2	Chameleon Constraints from Tests of Gravity	11
2.1.3	Observational Signatures	11
2.1.4	Cosmology of Chameleon Models	12
2.1.5	$f(R)$ Theories	13
2.2	Symmetron Fields	16
2.2.1	Symmetron Thin-Shell Screening	17
2.2.2	Tests of Gravity and Observational Signatures	18
2.3	Theories of Massive/Resonance Gravity	18
2.3.1	Fierz-Pauli Gravity and Its Discontents	19
2.3.2	Dvali-Gabadadze-Porrati Gravity	20
2.3.3	Degravitation	23
2.3.4	Cascading Gravity	26
3	Tests from Astronomical Observations	30
3.1	Early Universe Tests	30
3.2	Large-Scale Structure Tests	31
3.2.1	Metric and fluid perturbations	31
3.2.2	Quasi-static Newtonian Regime	33
3.2.3	Tests using Lensing, ISW and Dynamical Observables	34
3.2.4	The Nonlinear Regime: Power Spectra and Halo Properties	40
3.3	Summary of Current Astrophysical Constraints	41
3.4	Upcoming Surveys	42
4	Discussion	45
5	Acknowledgements	46

1. Introduction

Einstein's theory of general relativity (GR) has proven spectacularly successful over 90 years of experimental tests [1]. These tests range from millimeter scale tests in the laboratory to solar system tests and consistency with gravity wave emission by binary pulsars. Recently cosmological motivations for modifying gravity have renewed interest in testing GR on scales of galaxies and large-scale structure.

Over the last decade it has become clear that the energy contents of the universe pose a major puzzle, in that GR plus the Standard Model of particle physics can only account for about 4% of the energy density inferred from observations. By introducing dark matter and dark energy, which account for the remaining 96% of the total energy budget of the universe, cosmologists have been able to account for a wide range of observations, from the overall expansion of the universe to the large scale structure of the early and late universe [2].

The Λ -Cold Dark Matter (Λ CDM) paradigm has thus emerged as the standard model of cosmology. While its phenomenological success is undeniable, few would argue for its aesthetic appeal. The model requires introducing exotic components of matter and energy. And while the vacuum energy of quantum fields offers a natural candidate for dark energy, the predicted amplitude from field theory calculations is many orders of magnitude larger than inferred from observations [3].

A critical assumption in the standard picture is the validity of GR at galactic and cosmological scales. Since GR has not been tested independently on these scales, a natural alternative is that there are new gravitational degrees of freedom associated with the dark energy scale, and that these degrees of freedom are responsible for the observed late-time cosmic acceleration. This possibility, that modifications in GR at cosmological scales can replace dark matter and/or dark energy, has become an area of active research in recent years. See [4] and references therein. The driving motivation for many practitioners is of course the vexing problem of the cosmological constant, since any solution to this long-standing puzzle promises to have profound implications for the nature of cosmic acceleration.

This review article discusses the prospects of testing GR on the largest scales through cosmological observations. Doing so in a model-independent way is unfortunately not without ambiguities. Unlike solar system tests, where the matter stress-energy tensor is known (*i.e.*, the Sun), cosmological tests inherently rely on assumptions about the stress-energy composition of the universe — any modification to the gravitational side of Einstein’s equations can equivalently be interpreted as a dark energy contribution to the stress-energy side [5, 6, 7]. Throughout this paper, we assume that the dark energy component is nearly spatially-homogeneous. Thus strictly speaking the cosmological tests discussed below are in fact tests of the assumption of GR plus smooth dark energy. Fortunately, however, nearly all of the specific modifications discussed below also lead to testable deviations from GR in the solar system.

In the rest of this introductory section, we briefly review existing constraints on deviations from GR from solar system and laboratory tests of gravity. In Sec. 2 we review some of the leading proposals for modified gravity (MG) theories, designed as an alternative to dark energy to explain the present day acceleration of the universe. In these models gravity at late cosmic times and on large scales departs from the predictions of GR. Note that for the purpose of this review we do not discuss alternatives to dark matter, such as Modified Newtonian Dynamics (MOND) [8] and its Tensor-Vector-Scalar (TeVeS) covariant generalization [9, 10]. In Sec. 3 we consider the prospects of testing such models in view of the massive new astronomical surveys and other experiments expected in the coming decade. We conclude with brief remarks in Sec. 4.

1.1. Approaches to Modify Gravity

The field equations of GR can be derived from the action

$$S_{\text{GR}} = \frac{M_{\text{Pl}}^2}{2} \int d^4x \sqrt{-g} R + S_{\text{matter}}[g_{\mu\nu}], \quad (1)$$

where $M_{\text{Pl}}^2 = 1/8\pi G_{\text{N}}$ with G_{N} being Newton's gravitational constant, g is the determinant of the metric tensor $g_{\mu\nu}$, and R is the Ricci scalar. The first term is the Einstein-Hilbert action, while S_{matter} contains all matter fields, with minimal couplings to $g_{\mu\nu}$. The stationary point of the variation of S_{GR} with respect to the metric then yields the Einstein field equations.

The simplest and best-studied modifications to General Relativity are scalar-tensor theories, which introduce a scalar cousin to the graviton. First proposed by Brans and Dicke [11] as an attempt to reconcile gravity with Machian ideas [12, 13, 14, 15], scalar-tensor lagrangians are now understood to arise as low-energy limits of various theories of particle physics. These include dimensional reductions of higher-dimensional gravity and brane-world models [16, 17, 18, 19, 20, 21]. Moreover, a host of more intricate modifications of gravity, including massive gravity and the Dvali-Gabadadze-Porrati (DGP) model [22, 23, 24, 25], reduce to a scalar-tensor form in certain decoupling limits [26, 27, 28].

The Brans-Dicke action [11] is characterized by a universally-coupled scalar field,

$$S_{\text{BD}} = \frac{M_{\text{Pl}}^2}{2} \int d^4x \sqrt{-\tilde{g}} \left(\Phi \tilde{R} - \frac{\omega_{\text{BD}}}{\Phi} (\partial\Phi)^2 \right) + S_{\text{matter}}[\tilde{g}_{\mu\nu}]. \quad (2)$$

The effective Newton's constant is thereby promoted to a scalar field. The field redefinitions $g_{\mu\nu} = \Phi \tilde{g}_{\mu\nu}$ and $\phi = -M_{\text{Pl}} \sqrt{3/2 + \omega_{\text{BD}}} \log \Phi$ map (2) to the Einstein frame, where the coefficient of the Einstein-Hilbert term is constant:

$$S_{\text{BD}}^{\text{Einstein}} = \int d^4x \sqrt{-g} \left(\frac{M_{\text{Pl}}^2}{2} R - \frac{1}{2} (\partial\phi)^2 \right) + S_{\text{matter}} \left[g_{\mu\nu} e^{2\beta\phi/M_{\text{Pl}}} \right]. \quad (3)$$

For future use, we have introduced $2\beta \equiv 1/\sqrt{3/2 + \omega_{\text{BD}}}$. Unfortunately, as reviewed below, the Brans-Dicke parameter is so tightly constrained by solar system and pulsar observations, $\omega_{\text{BD}} \gtrsim 4 \times 10^4$ [1], that the cosmological effects of the scalar field are rendered uninterestingly small. Since this stringent constraint only applies to visible matter, many authors have relaxed the assumption of universal coupling and explored models in which the scalar field only substantially interacts with the dark matter [29, 30, 31, 32, 33, 34, 35, 36, 37].

The alternative gravity theories discussed in Sec. 2 all reduce to scalar-tensor theories in certain limits. (See [38], however, for an IR modification of gravity without new degrees of freedom.) To produce interesting effects cosmologically while satisfying the tight local constraints on deviations from GR, these scalar fields must somehow be hidden or screened in the local environment. There are three known mechanisms for screening a scalar field, all of which exploit the fact that the matter density at a typical location in the solar system or in pulsar environments is many orders of magnitude larger than the mean cosmic density. The success of these models relies on a nonlinear mechanism that operates on small scales or inside dense objects to recover GR on solar-system/pulsar scales where gravity is well tested. The large local background density triggers nonlinearities in the scalar field, which in turn result in its decoupling from matter. In short, the three mechanisms rely on giving the scalar field a large mass, a large inertia, or by weakening its coupling to matter, respectively.

The first mechanism, discussed in Sec. 2.1, arises in chameleon field theories [39, 40, 41, 42]. By adding a suitable self-interaction potential $V(\phi)$ to (3), the chameleon scalar field acquires mass which depends on the density. The mass is large in regions of high density, thereby suppressing any long-range interactions. (Density-dependent effective couplings were initially noted in a different context [43].) Chameleon fields can in fact have different couplings to different matter species, thereby generalizing the universal coupling assumed in Brans-Dicke theories. A subclass of chameleon theories are so-called $f(R)$ theories of gravity [44, 45, 46, 47, 48, 49, 50] — for $\omega_{\text{BD}} = 0$ and suitable choice of $V(\phi)$, the scalar-tensor action can be mapped through field redefinitions into an action of the form (1) with the Einstein-Hilbert term replaced by $f(R)$, a general function of the Ricci scalar.

The second mechanism for hiding a scalar is achieved with symmetron fields (Sec. 2.2), proposed recently in [51, 52]. The symmetron Lagrangian is qualitatively similar to that of chameleon models, but the mechanism and its phenomenological consequences are drastically different. The screening in this case relies on a scalar field acquiring a vacuum expectation value (VEV) that is small in high-density regions and large in low-density regions. An essential ingredient is that the coupling to matter is proportional to this VEV, so that the scalar couples with gravitational strength in low-density environments, but is decoupled and screened in regions of high density. This is achieved through a symmetry-breaking potential, hence the name symmetron.

The third mechanism, discussed in Sec. 2.3, relies on the scalar field having derivative interactions that become large in regions of high density or in the vicinity of massive objects. Perturbations of the scalar in such regions acquire a large kinetic term and therefore decouple from matter. Thus the scalar screens itself and becomes invisible to experiments. This so-called Vainshtein effect [53, 54, 55] ensures the phenomenological viability of brane-world modifications of gravity [22, 23, 24, 56, 57, 58, 59, 60, 61, 62, 63, 64, 65] and galileon scalar field theories [66, 67, 68, 69, 70, 71, 72].

These various theories and the corresponding observational constraints will be discussed respectively in Secs. 2 and 3. To set the stage for these discussions, we briefly review the current constraints on GR from laboratory and solar system tests of gravity. For a more detailed review of the subject, see [1].

1.2. Newtonian Tests

Einstein's gravity theory is based on the weak equivalence principle (WEP), which states that the trajectory of a freely falling test body is independent of its internal structure and composition. The WEP is of course not unique to GR — any theory whose matter fields couple to a unique metric tensor, *e.g.* the Brans-Dicke theory in (2), satisfies the WEP, independent of the field equations governing this metric. (As we review below, scalar-tensor theories, including Brans-Dicke, violate a stronger version of the equivalence principle satisfied in GR — the Strong Equivalence Principle (SEP) — which extends the universality of free-fall to include gravitational self-energy contributions.)

Eötvös-type experiments test the WEP by measuring the η parameter — the fractional difference in the acceleration of freely falling bodies of different composition. The best limit comes from the torsion balance experiment of the University of Washington (Eöt-Wash), which gives $\eta = (0.3 \pm 1.8) \times 10^{-13}$ [73]. The forthcoming space-based mission MicroSCOPE [74] is designed to reach 10^{-15} sensitivity. Other satellite experiments, such as Galileo Galilei [75] and the Satellite test of the Equivalence Principle (STEP) [76], will further improve on current limits.

Even when the WEP is satisfied, modifications of gravity are also constrained by tests of the gravitational inverse-square law [77]. The simplest example is a scalar field with mass m mediating a force of range λ and coupling strength α , corresponding to the Yukawa potential

$$\psi = -\alpha \frac{G_{\text{N}}M}{r} e^{-r/\lambda} \quad (4)$$

Experimental tests can be characterized as providing limits on λ and α [73, 78, 79]. For gravitational-strength coupling ($\alpha \sim \mathcal{O}(1)$), there is no evidence of a fifth force down to $\lambda = 56 \mu\text{m}$ [78].

1.3. Post-Newtonian Tests

The early experimental successes of GR were the consistency with the perihelion shift of Mercury and the deflection of light by the Sun. Beginning around 1960, a number of experimental tests of GR were carried out, including the measurement of gravitational redshift. The consistency of the decrease in the orbital period of the Hulse-Taylor binary pulsar with the GR prediction of energy loss due to gravity waves further established the validity of GR in the weak field regime.

Solar system tests of alternate theories of gravity are commonly phrased in the language of the Parameterized Post-Newtonian (PPN) formalism. The PPN formalism applies to metric theories of gravity in the weak field, slow motion limit, *i.e.* when potentials and velocities are small: $\Psi, v^2/c^2 \sim \epsilon^2 \ll 1$. The metric can then be written as a perturbation about the Minkowski metric (or, as we shall see, the FRW metric for the expanding universe). Terms up to second order in the potentials are included, with coefficients that are unity or zero for GR replaced by parameters that accommodate MG theories.

The γ and β PPN parameters are given by the metric

$$ds^2 = -(1 + 2\Psi - 2\beta\Psi^2) dt^2 + (1 - 2\gamma\Psi) d\vec{x}^2 \quad (5)$$

where the potential $\Psi = -G_{\text{N}}M/r$ for the Schwarzschild metric. The parameter γ describes the spacetime curvature induced by a unit mass and β the nonlinearity in the superposition law of gravity. We will employ a similar metric in Sec. 3 with the FRW metric and an arbitrary (small) potential. In general for a fluid description of matter, allowing for generic Poisson-like potentials, the PPN formalism requires ten parameters for a complete description [1]. Note that the PPN formalism has constant parameters and therefore does not accommodate

Yukawa-like modifications with finite λ . For astrophysical tests we will work with effective parameters that may have a scale and time dependence, but a similar expansion of the metric is still useful.

The Brans-Dicke theory given by (2) has identical PPN parameter values as in GR, except for $\gamma = (1 + \omega_{\text{BD}})/(2 + \omega_{\text{BD}})$. Since γ is the most relevant PPN parameter for the modified gravity theories of interest, we focus on this parameter for the rest of our discussion.

The tightest constrain on γ comes from time-delay measurements in the solar system, specifically the Doppler tracking of the Cassini spacecraft, which gives $\gamma - 1 = (2.1 \pm 2.3) \times 10^{-5}$ [80]. Light deflection measurements, meanwhile, constrain γ at the 10^{-4} level [81]. The observed perihelion shift of Mercury's orbit sets a weaker limit of 10^{-3} [82].

As mentioned earlier, GR satisfies an extended version of the equivalence principle, the SEP, which states, in particular, that macroscopic objects follow the same trajectory in a uniform gravitational field as test masses. In other words, the universality of free-fall is preserved in GR even when accounting for self-gravity contributions. The SEP is violated in Brans-Dicke theories and in all of the MG theories considered here. Violations of the SEP result in the Nordtvedt effect [83] — a difference in the free-fall acceleration of the Earth and the Moon towards the Sun, which is detectable in Lunar Laser Ranging (LLR). (Because the Earth and the Moon have different compositions, however, one must worry about a fluke cancellation between WEP and SEP violations in this measurement. To disentangle these effects, laboratory tests of the WEP have been performed using test masses with Earth-like and Moon-like compositions [84].) Searches for the Nordtvedt effect in LLR data constrain PPN deviations from GR at the 10^{-4} level [1].

2. Modified Gravity Theories

In this Section we review various proposals for modifying GR at large distances. The list is by no means exhaustive — our goal is to provide the reader with an overview of a few broad classes of theories that have attracted considerable interest over the last few years, highlighting key theoretical and observational differences among them. For this purpose, we find it useful to group theories based on the three qualitatively different non-linear mechanisms through which GR is approximately recovered locally. These are the chameleon (Sec. 2.1), Vainshtein (Sec. 2.3) and symmetron (Sec. 2.2) mechanisms.

2.1. Chameleon/ $f(R)$ Field Theories

Chameleon field theories generalize (3) to include a scalar potential $V(\phi)$, whose properties will be discussed shortly, as well as a more general coupling $A(\phi)$ to matter fields:

$$S_{\text{cham}} = \int d^4x \sqrt{-g} \left(\frac{M_{\text{Pl}}^2}{2} R - \frac{1}{2} (\partial\phi)^2 - V(\phi) \right) + S_{\text{matter}} [g_{\mu\nu} A^2(\phi)] . \quad (6)$$

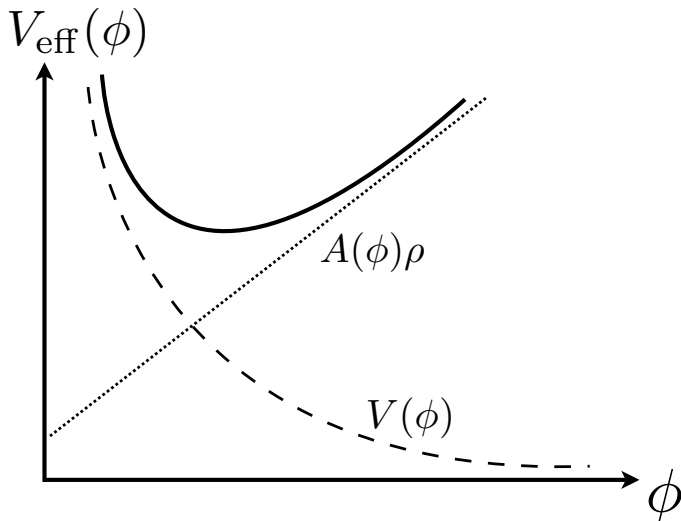


Figure 1: The chameleon effective potential V_{eff} (solid curve) is the sum of two contributions: the actual potential $V(\phi)$ (dashed curve), plus a density-dependent term from its coupling to matter (dotted curve).

One can allow different couplings to the various matter fields, thereby introducing violations of the Equivalence Principle. Furthermore, one can also introduce a coupling to the electromagnetic field strength, which induces photon-chameleon mixing in the presence of magnetic fields [85, 86]. For the purpose of this review article, we focus on the simplest case of a universal, conformal coupling of the chameleon, as in (6).

The equation of motion for ϕ that derives from this action is

$$\square\phi = V_{,\phi} - A^3(\phi)A_{,\phi}\tilde{T}, \quad (7)$$

where $\tilde{T} = \tilde{g}_{\mu\nu}\tilde{T}^{\mu\nu}$ is the trace of the energy-momentum tensor defined with respect to the Jordan-frame metric $\tilde{g}_{\mu\nu} = A^2(\phi)g_{\mu\nu}$. Since matter fields couple minimally to $\tilde{g}_{\mu\nu}$, this stress tensor is covariantly conserved: $\tilde{\nabla}_\mu\tilde{T}^{\mu\nu} = 0$.

To study the field profile on solar system and galactic scales, we can approximate the metric in (7) as flat space, ignore time derivatives, and focus on the case of a non-relativistic, pressureless source. In terms of an energy density $\rho = A^3(\phi)\tilde{\rho}$ conserved in Einstein frame, we obtain

$$\nabla^2\phi = V_{,\phi} + A_{,\phi}\rho. \quad (8)$$

Thus, because of its coupling to matter fields, the scalar field is affected by ambient matter density. Its profile is governed by an effective potential

$$V_{\text{eff}}(\phi) = V(\phi) + A(\phi)\rho. \quad (9)$$

For suitably chosen $V(\phi)$ and $A(\phi)$, this effective potential can develop a minimum at some finite field value ϕ_{\min} in the presence of background matter density, as illustrated in Fig. 1, where the mass of the chameleon field is sufficiently large to evade local constraints:

$$m_{\min}^2 = V_{,\phi\phi}(\phi_{\min}) + A_{,\phi\phi}(\phi_{\min})\rho. \quad (10)$$

Assuming $A(\phi)$ is monotonically increasing, for concreteness, the general conditions that $V(\phi)$ must satisfy are [39, 87]: (i) to balance the potential against the density term, we must have $V_{,\phi} < 0$ over the relevant field range; (ii) since $V_{,\phi\phi}$ typically gives the dominant contribution to the mass term, stability requires $V_{,\phi\phi} > 0$; (iii) the effective mass increases with density provided that $V_{,\phi\phi\phi} < 0$.

As seen from Fig. 1, for suitable choices of V and A , the effective mass can be a steeply growing function of the ambient density. The chameleon mechanism therefore exploits the large difference between local ($\sim 1 \text{ g/cm}^3$) and cosmic ($\approx 10^{-30} \text{ g/cm}^3$) densities to generate a wide range in mass scales. As we have seen in Sec. 1.2, tests of the inverse-square law constrain the range in the laboratory to be $\lesssim 50 \mu\text{m}$. Meanwhile, we would ideally like to achieve $m_{\text{eff}} \sim H_0$ at cosmological densities, such that the chameleon behaves as a quintessence field. In all known examples, however, the best one can do is $m_{\text{eff}} \gtrsim 10^4 H_0$, corresponding to a range $\lesssim 0.1 \text{ Mpc}$ in the cosmos. The reason for this is simple — for a potential for which $m_{\text{eff}} \sim H_0$ at cosmological densities, the field value where this is reached is generally a distance $\sim M_{\text{Pl}}$ away from the local value, and maintaining gradient of such a large field difference is just energetically too costly. The largest gradient energy that can be tolerated corresponds in practice to $m_{\text{eff}} \gtrsim 10^4 H_0$ at cosmological densities.

A prototypical potential that satisfies all of the above conditions is the inverse power-law form,

$$V(\phi) = \frac{M^{4+n}}{\phi^n}, \quad (11)$$

where n is some positive constant. This falls within the class of tracker potentials relevant for quintessence models of dark energy [88]. For the coupling function, a nice choice that makes contact with Brans-Dicke theories is the exponential form of (3):

$$A(\phi) = e^{\beta\phi/M_{\text{Pl}}}. \quad (12)$$

The parameter β is implicitly assumed to be $\mathcal{O}(1)$, corresponding to gravitational strength coupling. Remarkably, it was pointed out in [42] that much larger couplings are allowed by current constraints, but one must be concerned with adiabatic instabilities for $\beta \gg 1$ [89]. Assuming $\beta\phi \ll M_{\text{Pl}}$, which will be the case for most situations of interest, the effective minimum lies at

$$\phi_{\min} \approx \left(\frac{nM^{4+n}M_{\text{Pl}}}{\beta\rho} \right)^{\frac{1}{n+1}}. \quad (13)$$

Meanwhile, the mass of small fluctuations around this value is

$$m_{\min}^2 \approx n(n+1)M^{-\frac{4+n}{1+n}} \left(\frac{\beta\rho}{nM_{\text{Pl}}} \right)^{\frac{n+2}{n+1}}. \quad (14)$$

Both ϕ_{\min} and m_{\min} manifestly depend on the matter density — m_{\min} grows larger for increasing ρ , as desired, while ϕ_{\min} decreases.

Potentials with *positive* powers of the field, $V(\phi) \sim \phi^{2\alpha}$ with α an integer ≥ 2 , are also good candidates for chameleon theories. In the simplest case of $V(\phi) = \lambda\phi^4$, [40] showed that existing laboratory constraints at the time were satisfied for $\beta = 1$ and $\lambda = 1$. Moreover, the authors of [40] identified various signatures for future laboratory tests of the inverse-square-law. Subsequent analysis by the Eöt-Wash group [79] excluded a significant part of the parameter space.

2.1.1. Thin-Shell Screening

The density-dependent mass immediately results in a further decoupling effect outside sufficiently massive objects, due to the *thin-shell* effect. Consider a spherical source of radius R and density ρ_{in} embedded in a homogeneous medium of density ρ_{out} . The corresponding effective minima will be respectively denoted by $\phi_{\text{min-in}}$ and $\phi_{\text{min-out}}$. For a sufficiently massive source, the scalar field is oblivious to the exterior matter and is therefore pinned near $\phi_{\text{min-in}}$ in the core of the object. Of course, ϕ must deviate substantially from $\phi_{\text{min-in}}$ near the surface of the object since ϕ must eventually reach the asymptotic value $\phi_{\text{min-out}}$ far away. Thus the gradient in ϕ builds up only within a thin-shell of thickness ΔR below the surface, given by

$$\frac{\Delta R}{R} = \frac{1}{6\beta M_{\text{Pl}}} \frac{\phi_{\text{min-out}} - \phi_{\text{min-in}}}{\Phi_{\text{N}}}, \quad (15)$$

where Φ_{N} is the surface Newtonian potential. In other words, the shell thickness is determined by the difference in ϕ values relative to the difference in gravitational potential between the surface and infinity.

Since field gradients are essentially confined to the shell, the exterior profile is suppressed by a thin-shell factor:

$$\phi_{\text{screen}} \approx -\frac{\beta}{4\pi M_{\text{Pl}}} \frac{3\Delta R}{R} \frac{M e^{-m_{\text{min-out}} r}}{r} + \phi_{\text{min-out}}. \quad (16)$$

The suppression factor of $\Delta R/R$ can alternatively be understood in a more intuitive way as follows. Deep inside the source, the contribution to the exterior profile from infinitesimal volume elements are Yukawa-suppressed due to the large effective chameleon mass in the core. Only the flux lines from within the thin-shell can propagate nearly unsuppressed to an exterior probe.

Clearly the thin-shell screening breaks down for sufficiently small objects. Imagine shrinking the source radius keeping the density fixed. Eventually, the cost in gradient energy to maintain the field difference between $\phi_{\text{min-in}}$ and $\phi_{\text{min-out}}$ becomes too large, and the scalar field no longer reaches $\phi_{\text{min-in}}$ in the core of the object. In this limit the thin-shell screening goes away, and the exterior profile takes its usual form

$$\phi_{\text{no screen}} \approx -\frac{\beta}{4\pi M_{\text{Pl}}} \frac{M e^{-m_{\text{min-out}} r}}{r} + \phi_{\text{min-out}}. \quad (17)$$

The criterion for thin-shell screening to be effective is for the right-hand side of (15) to be $\ll 1$. Clearly, the more massive the source, the easier is this condition satisfied, as expected. But note that the criterion also depends on the density contrast — for fixed source, a denser environment implies smaller $\phi_{\text{min-out}}$, which makes the thin-shell condition easier to satisfy. We will see in Sec. 2.1.3 that the thin-shell screening effect leads to striking observational signatures.

2.1.2. Chameleon Constraints from Tests of Gravity

The tightest constraint on the model comes from fifth-force searches in the laboratory [77], which set a limit of $\approx 50 \mu\text{m}$ [78] on the fifth-force range for gravitational strength coupling. Modeling the chameleon profile in the Eöt-Wash set-up, taking into account that torsion-balance measurements are performed in vacuum, it was shown in [39] that, for the inverse power-law potential $V(\phi) = M^{4+n}/\phi^n$ with n and β of order unity, the fifth-force constraint translates into a bound on M :

$$M \lesssim 10^{-3} \text{ eV}. \quad (18)$$

Remarkably, the upper bound coincides with the energy scale of dark energy: $\Lambda \sim (10^{-3} \text{ eV})^4$. This bound not only ensures that the chameleon is consistent with fifth force searches, but it is also sufficient to satisfy all known tests of GR (see Secs. 1.2 and 1.3), such as searches for WEP violation, Lunar Laser Ranging observations and other tests of post-Newtonian gravity [39, 40].

2.1.3. Observational Signatures

Because objects of different mass have different effective coupling to the scalar, macroscopic violations of the Equivalence Principle can arise, even in the case where the microphysical lagrangian (6) displays no such violations [39, 40, 90]. In particular, test masses that are screened in the laboratory may not be screened in space. This leads to the striking prediction that satellite tests of gravity, such as the planned MicroSCOPE [74], Galileo Galilei [75] and STEP [76] missions, might observe violations of the WEP with $\eta \gg 10^{-13}$, in blatant conflict with laboratory constraints. Meanwhile, from (17) the total force (gravitational + chameleon-mediated) between unscreened particles is a factor of $1 + 2\beta^2$ larger than gravity, which would appear as $\mathcal{O}(1)$ deviations from G_N measured on Earth.

Effective violations of the WEP also results in a host of astrophysical signatures uncovered in [90]. For example, consider (unscreened) dwarf galaxies in large void regions. The HI gas in these galaxies is also unscreened, but the stars are screened. This should result in a systematic $\mathcal{O}(1)$ mismatch in the rotational velocities of these two tracers, and hence a corresponding mismatch in mass estimates.

Other interesting observable signals arise if the chameleon couples to the electromagnetic field

$$\int d^4x \sqrt{-g} e^{\beta\gamma\phi/M_{\text{Pl}}} F_{\mu\nu} F^{\mu\nu}. \quad (19)$$

Such a coupling results in photon-chameleon oscillations in the presence of an external magnetic field. The GammeV experiment [91, 92, 93] searches for the afterglow [94, 95] that would result from trapped chameleons converting back into photons and has so far excluded the range $5 \times 10^{11} < \beta < 6.4 \times 10^{12}$ [91]. This bound has been further refined recently in a more complete analysis [93]. The second-generation experiment, GammeV-CHASE, is currently taking data and will further improve on this bound [93]. Photon-chameleon mixing can also be detected astrophysically, through induced polarization in the spectrum of astrophysical objects [96] and enhanced scatter in the X/ γ -ray luminosity relation of active galactic nuclei (AGN) [97]. A recent analysis of AGN data shows tantalizing evidence of this effect [97].

2.1.4. Cosmology of Chameleon Models

The chameleon scalar field can act as dark energy driving cosmic acceleration. Unfortunately the bound (18) from local tests of gravity forces the equation of state of the chameleon component to be indistinguishable from $w = -1$, resulting in an expansion history identical to Λ CDM. This is closely related to a point made earlier: in order to generate observable deviations from $w = -1$, the chameleon field must be rolling significantly on a Hubble time, which requires $m_{\text{eff}} \sim H_0$ on cosmological scales. But this in turn requires a field displacement of order M_{Pl} from the local value to the cosmos, which is too costly energetically — galaxies can no longer maintain their thin shell, leading to gross violations of local constraints.

Explicitly, the inverse power-law form, $V(\phi) = M^{4+n}/\phi^n$, leads to too small a dark energy contribution for $M \sim 10^{-3}$ eV. In order to account for cosmic acceleration, we must lift this potential by an appropriate constant, which of course has no effect on our earlier analysis of local tests. We can exploit the coincidence of the dark energy scale and the upper bound in (18) to choose a potential with a single mass parameter [41]

$$V(\phi) = M^4 \exp(M^n/\phi^n), \quad (20)$$

with $M = 10^{-3}$ eV. For $\phi \gg M$, this gives $V(\phi) \approx M^4 + M^{4+n}/\phi^n + \dots$, which is (11) plus a constant. Thus, while cosmic acceleration is not explained in chameleon models, it is easily incorporated within its phenomenology.

Let us now turn to the cosmological evolution of the chameleon. In the matter-dominated era, (7) reduces to

$$\ddot{\phi} + 3H\dot{\phi} = -V_{,\phi} - A_{,\phi}\rho_m, \quad (21)$$

where ρ_m satisfies the usual conservation law: $\dot{\rho}_m + 3H\rho_m = 0$. In particular, the effective potential for ϕ is time-dependent. The behavior of the scalar can be inferred by standard adiabaticity arguments — as long as $m_{\text{min}} \gg H$, the field continuously adjusts to the evolving minimum. This is manifestly satisfied for the potential (20) and coupling function (12),

$$\frac{m_{\text{min}}^2}{H^2} \approx 3\beta \Omega_m \frac{M_{\text{Pl}}}{\phi_{\text{min}}} \left\{ 1 + n + n \left(\frac{M}{\phi_{\text{min}}} \right)^n \right\} \gg 1, \quad (22)$$

since $\phi_{\min} \ll M_{\text{Pl}}$ for relevant densities, as mentioned earlier. The fact that $m(\phi_{\min}) \gg H$ on cosmological scales today is yet another way of seeing that chameleon dark energy is indistinguishable from a cosmological constant at the background level.

The story is more subtle in the radiation-dominated era, since $\tilde{T}^\mu_\mu \approx 0$ for a relativistic fluid, and hence the source term in (7) vanishes. This suggests that the field is overdamped and remains frozen until matter-radiation equality, which would lead to inconsistencies with nucleosynthesis if the field started out in the early universe with generic initial displacement $\sim M_{\text{Pl}}$. Fortunately, the trace is not always small for a realistic relativistic fluid. As the universe expands and cools, matter species in the thermal bath successively become non-relativistic when $m \sim T$. Whenever this happens, \tilde{T}^μ_μ becomes non-zero for about one e-fold of expansion, until the species in question becomes Boltzmann suppressed, thus driving the field closer to the minimum [98]. The total displacement incurred by “kicks” from known particles until nucleosynthesis is of order βM_{Pl} [41]. Thus, for a broad range of initial conditions the field settles to the effective minimum by the onset of nucleosynthesis.

2.1.5. $f(R)$ Theories

A class of chameleon theories that has sparked considerable interest over the last few years is the $f(R)$ form [44, 45], where the Einstein-Hilbert term in (1) is replaced by a general function of the Ricci scalar [44, 45, 46]:

$$S = \frac{M_{\text{Pl}}^2}{2} \int d^4x \sqrt{-\tilde{g}} f(\tilde{R}) + S_{\text{matter}}[\tilde{g}_{\mu\nu}]. \quad (23)$$

See [47, 48] for recent reviews. This action was first introduced by Starobinsky in the context of inflation [99] and studied further in [100, 101, 102]. Functions of other curvature invariants have also been considered [103], but this generally introduces ghost instabilities [104]. (Of course general higher-order curvature invariants are harmless from an effective field theory point of view provided they contribute small corrections to Einstein gravity. But here one is precisely interested in order-unity deviations from General Relativity.) The only exceptions are functions of the Ricci scalar (as in (23)) or functions of the Gauss-Bonnet term [105].

It is well-known that (23) is just a scalar-tensor theory in another guise. To see this, introduce a non-dynamical scalar ψ :

$$S = \frac{M_{\text{Pl}}^2}{2} \int d^4x \sqrt{-\tilde{g}} \left\{ f(\psi) + \frac{df}{d\psi} (\tilde{R} - \psi) \right\} + S_{\text{matter}}[\tilde{g}_{\mu\nu}]. \quad (24)$$

Varying with respect to ψ imposes the constraint $\psi = R$, assuming $f'' \neq 0$. And since the constraint is algebraic, we can substitute it back into (24), thereby reproducing (23). Furthermore, the field redefinitions $g_{\mu\nu} = (df/d\psi)\tilde{g}_{\mu\nu}$ and $\phi = -\sqrt{3/2}M_{\text{Pl}} \log df/d\psi$ reduce (24) to the more familiar form

$$S = \int d^4x \sqrt{-g} \left(\frac{M_{\text{Pl}}^2}{2} R - \frac{1}{2} (\partial\phi)^2 - V(\phi) \right) + S_{\text{matter}} \left[g_{\mu\nu} e^{\sqrt{2/3}\phi/M_{\text{Pl}}} \right], \quad (25)$$

where the only remnant of the $f(R)$ choice is encoded in the scalar potential:

$$V = \frac{M_{\text{Pl}}^2 \left(\psi \frac{df}{d\psi} - f \right)}{2 \left(\frac{df}{d\psi} \right)^2}. \quad (26)$$

The action (25) is precisely of the form (6). Theories of $f(R)$ gravity are therefore physically equivalent to a subclass of chameleon field theories, namely those with $A(\phi)$ given by (12) for the specific choice $\beta = 1/\sqrt{6}$, as can be seen from (25). In other words, only for this specific choice of β do chameleon theories allow an $f(R)$ description.

For completeness, we give the equations of motion in the $f(R)$ language. Varying (24) with respect to the metric gives the modified Einstein field equations

$$G_{\mu\nu} + f_{,R} R_{\mu\nu} - \left(\frac{f}{2} - \square f_{,R} \right) g_{\mu\nu} - \nabla_\mu \nabla_\nu f_{,R} = 8\pi G_{\text{N}} T_{\mu\nu}, \quad (27)$$

where $T_{\mu\nu} = -(2/\sqrt{-g})\delta S_{\text{matter}}/\delta g^{\mu\nu}$ is the matter stress-energy tensor, and $f_{,R} \equiv df/dR$. Taking the trace of (27) yields an equation for the scalar degree of freedom $f_{,R}$:

$$\square f_{,R} = \frac{1}{3} (R - f_{,R} R + 2f + 8\pi G_{\text{N}} T^\mu{}_\mu). \quad (28)$$

Two popular choices of $f(R)$ are the Hu-Sawicki [49] and Starobinsky [50] forms, given respectively by

$$f(R) = R - \frac{aM^2}{1 + \left(\frac{R}{M^2}\right)^{-\alpha}} \quad (\text{HS}); \quad (29)$$

$$f(R) = R + aM^2 \left[\left(1 + \frac{R^2}{M^4}\right)^{-\alpha/2} - 1 \right] \quad (\text{S}), \quad (30)$$

where a and α are positive constants. (For convenience we have redefined the parameters of [49] as follows: $M^2 = m^2/c_2^{1/n}$, $a = c_1 c_2^{-1+1/n}$.) Both forms satisfy $f(R) \rightarrow 0$ as $R \rightarrow 0$. For the relevant choices of parameters, however, the entire cosmological history of our universe lies in the $R \gg M^2$ regime, in which both forms have identical limits:

$$f(R) \approx R + aM^2 \left[-1 + \left(\frac{R}{M^2}\right)^{-\alpha} \right] \quad (R \gg M^2). \quad (31)$$

In particular, this is the relevant regime to describe the chameleon mechanism. Using the above dictionary, the corresponding potential for the canonically-normalized scalar field in Einstein frame is

$$V(\phi) \approx \frac{a}{2} M^2 M_{\text{Pl}}^2 \left\{ 1 - (\alpha + 1) \left(\sqrt{\frac{2}{3}} \frac{1}{\alpha a} \frac{\phi}{M_{\text{Pl}}} \right)^{\frac{\alpha}{\alpha+1}} \right\}. \quad (32)$$

This potential is finite at $\phi = 0$ (corresponding to $R \rightarrow \infty$ in the $f(R)$ language), but its derivative blows up at this point for any $\alpha > 0$. This is a generic consequence of starting with a nice functional form in the $f(R)$ language — translating to the scalar-tensor language involves inverting a relation to obtain $R = R(\phi)$, which therefore typically results in a non-analytic scalar potential.

The pathological form of the potential is indicative that quantum corrections become important near $\phi = 0$ [106]¹. The scalar potential $V(\phi)$ receives radiative corrections from ϕ loops, whose finite part at 1-loop is

$$\Delta V_{1\text{-loop}} = \frac{V_{,\phi\phi}^2}{64\pi^2} \log\left(\frac{V_{,\phi\phi}}{\mu^2}\right) \sim \left(\frac{\phi}{M_{\text{Pl}}}\right)^{-2\frac{\alpha+2}{\alpha+1}} \log\left(\frac{\phi^2}{\mu^2}\right), \quad (33)$$

(As usual there are also divergent pieces that must be fine-tuned to zero.) This overwhelms the classical part for $\phi \ll M_{\text{Pl}}$. Thus scalar configurations in the small-field limit are in the quantum regime in this case.

The cuspy form of the potential leads to pathologies already at the classical level [107, 108, 109]: although the static chameleon solutions described earlier only rely on $V_{,\phi}$ becoming large, the fact that V itself remains finite at $\phi = 0$ implies that finite-energy configurations (*e.g.* a collapsing star) can dynamically overshoot the effective minimum and hit the singular point. The singularity at $\phi = 0$ also led [110] to argue against the existence of relativistic stars in $f(R)$ gravity, though this conclusion has been questioned recently by [111]. What (33) shows, however, is that the classical approximation is not valid for $\phi \ll M_{\text{Pl}}$ — the $f(R)$ dynamics are dominated by quantum effects in this regime.

We should stress that these problems are specific to cuspy potentials of the form (32). The inverse power-law form of (11), for instance, is clearly immune to singularity issues. If a dynamical configuration causes the field to overshoot, the infinite barrier at $\phi = 0$ will stop the field and lead to oscillations around the minimum. (Alternatively, in [112, 113] it was shown that adding higher-order curvature invariants to (31) can remove the singular point and push the high-curvature regime to infinity in field space.) Similarly, the 1-loop contribution (33) can be under control over the relevant field range in this case [106].

What choice of $f(R)$ leads to inverse power-law potential? In the strong curvature regime, the desired form is

$$f(R) = R - aM^2 \left[1 + aM^2 \left(\frac{R}{M^2} \right)^{\frac{n}{1+n}} \right] \quad (R \gg M^2). \quad (34)$$

This is similar to (31), except that the power is positive in this case. Moreover, whereas (31) can be an analytic function of R , the above has branch cuts for any choice of n . As mentioned earlier, this is an unavoidable consequence of translating between the $f(R)$ and scalar-tensor forms — analytic $V(\phi)$'s map

¹We are grateful to Andrew Tolley for helpful discussions on this point.

onto non-analytic $f(R)$'s, and vice versa. The stability discussion above therefore implies that non-analytic dependence on the field variables is forced upon us if we insist on working in the $f(R)$ description.

2.2. Symmetron Fields

A second mechanism for hiding scalar fields was proposed recently in the context of symmetron field theories [51, 52]. As we will shortly, the symmetron technology and building blocks are similar to those of chameleon models. But the physics of the screening mechanism and its phenomenological consequences are dramatically different. In particular, unlike in chameleon theories, the symmetron has a small mass everywhere and therefore mediates a long-range force on Earth and in the solar system.

In the symmetron mechanism, the vacuum expectation value (VEV) of the scalar depends on the local mass density, becoming large in regions of low mass density, and small in regions of high mass density. In addition, the coupling of the scalar to matter is proportional to the VEV, so that the scalar couples with gravitational strength in regions of low density, but is decoupled and screened in regions of high density.

The starting point is the general chameleon action (6). In particular, we assume that the symmetron couples universally to matter fields through a conformal coupling. The scalar potential is of the symmetry-breaking form,

$$V(\phi) = -\frac{1}{2}\mu^2\phi^2 + \frac{1}{4}\lambda\phi^4, \quad (35)$$

involving a tachyonic mass scale μ and dimensionless coupling λ . Meanwhile, the coupling to matter is governed by

$$A(\phi) = 1 + \frac{1}{2M^2}\phi^2 + \mathcal{O}(\phi^4/M^4). \quad (36)$$

The field range of interest is restricted to $\phi \ll M$, as we will see shortly, thus higher-order terms in $A(\phi)$ are negligible. The theory described by (35) and (36) has a \mathbb{Z}_2 symmetry $\phi \rightarrow -\phi$. The self-interaction potential is the most general renormalizable form consistent with this symmetry. The quadratic coupling to the matter stress tensor is the leading such coupling compatible with the \mathbb{Z}_2 symmetry. It is non-renormalizable, suppressed by the mass scale M .

The screening mechanism is achieved through an interplay between the symmetry-breaking potential and the universal coupling to matter. In the case of a non-relativistic source, the effective potential (9) is given by

$$V_{\text{eff}}(\phi) = \frac{1}{2} \left(\frac{\rho}{M^2} - \mu^2 \right) \phi^2 + \frac{1}{4} \lambda \phi^4. \quad (37)$$

Thus, whether the quadratic term is negative or not, and hence whether the \mathbb{Z}_2 symmetry is spontaneously broken or not, depends on the local matter density. In vacuum, the potential breaks the reflection symmetry spontaneously, and the scalar acquires a vacuum expectation value (VEV) $\phi_0 \equiv \mu/\sqrt{\lambda}$. Inside a source

of sufficient density, such that $\rho > M^2\mu^2$, the effective potential no longer breaks the symmetry, and the VEV goes to zero.

An essential feature is that the lowest order coupling of matter to the symmetron is $\sim \rho\phi^2/M^2$. Fluctuations $\delta\phi$ around a local background value ϕ_{VEV} , as would be detected by local experiments, therefore couple as

$$\sim \frac{\phi_{\text{VEV}}}{M^2} \delta\phi \rho, \quad (38)$$

that is, the coupling is proportional to the local VEV. In high-density, symmetry-restoring environments, the VEV should be near zero, and fluctuations of ϕ should not couple to matter. In rarified environments, where $\rho < M^2\mu^2$, the symmetry is broken and the coupling turns back on.

The case of interest is where the field becomes tachyonic around the current cosmic density: $H_0^2 M_{\text{Pl}}^2 \sim \mu^2 M^2$. This fixes μ in terms of M , and hence the mass m_0 of small fluctuations around $\phi_0 = \mu/\sqrt{\lambda}$:

$$m_0 = \sqrt{2}\mu \sim \frac{M_{\text{Pl}}}{M} H_0. \quad (39)$$

Local tests of gravity, as we will see, require $M \lesssim 10^{-3} M_{\text{Pl}}$. Hence the range m_0^{-1} of the symmetron-mediated force in vacuum is \lesssim Mpc. Meanwhile, if this extra force is to be comparable in strength to the gravitational force in vacuum, then from (38) we must impose $\phi_0/M^2 \sim 1/M_{\text{Pl}}$, that is,

$$\phi_0 \equiv \frac{\mu}{\sqrt{\lambda}} \sim \frac{M^2}{M_{\text{Pl}}}. \quad (40)$$

Together with (39), this implies $\lambda \sim M_{\text{Pl}}^4 H_0^2 / M^6 \ll 1$. (For $M = 10^{-3} M_{\text{Pl}}$, in particular, this gives $\lambda = 10^{-102}$ — the symmetron is extremely weakly coupled.) We see immediately from (40) that $\phi_0 \ll M$, hence the field range of interest lies within the regime of the effective field theory, and $\mathcal{O}(\phi^4/M^4)$ corrections in (36) can be consistently neglected.

2.2.1. Symmetron Thin-Shell Screening

Symmetron solutions around a source display a thin-shell effect analogous to the chameleon behavior discussed in Sec. 2.1.1. Consider once again the ideal case of a static, spherically-symmetric source of homogeneous density $\rho > \mu^2 M^2$. For simplicity, we further assume the object lies in vacuum, so that the symmetron tends to its symmetry-breaking VEV far away: $\phi \rightarrow \phi_0$ as $r \rightarrow \infty$.

For a sufficiently massive source, in a sense that will be made precise shortly, the solution has the following qualitative behavior. Deep in the core of the object, the symmetron is weakly coupled to matter, since the matter density forces $\phi \approx 0$ there. Near the surface, meanwhile, the field must grow away from $\phi = 0$ in order to asymptote to the symmetry-breaking VEV far away. The symmetron is thus weakly coupled to the core of the object, and its exterior profile is dominated by the surface contribution. In other words, analogously to chameleon

models, there is a thin shell screening effect suppressing the symmetron force on an external test particle.

The parameter that determines whether a solution is screened or not is

$$\alpha \equiv \frac{\rho R^2}{M^2} = 6 \frac{M_{\text{Pl}}^2}{M^2} \Phi_{\text{N}}. \quad (41)$$

(Recall that Φ_{N} is the surface gravitational potential.) Objects with $\alpha \gg 1$ display thin-shell screening, and the resulting symmetron-mediated force on a test particle is suppressed by $1/\alpha$ compared to the gravitational force. Objects with $\alpha \ll 1$, on the other hand, do not have a thin shell — the symmetron gives an $\mathcal{O}(1)$ correction to the gravitational attraction in this case.

2.2.2. Tests of Gravity and Observational Signatures

Since the symmetron-mediated force is long-range in all situations of interest, and because the symmetron couples to matter universally, the relevant tests of gravity are the same that constrain standard BD theories: solar system and binary pulsar observations. A necessary condition is for the Milky Way galaxy to be screened: $\alpha_{\text{G}} \gtrsim 1$. Since $\Phi \sim 10^{-6}$ for the galaxy, (41) implies

$$M \lesssim 10^{-3} M_{\text{Pl}}. \quad (42)$$

It turns out that this condition is also sufficient to satisfy all current constraints. Indeed, as shown in [51], with $M = 10^{-3} M_{\text{Pl}}$ the symmetron predictions for time-delay, light-deflection, perihelion precession of Mercury and Nordvedt effect are comparable to current sensitivity levels and therefore detectable by next-generation experiments. Note that pushing M to larger values is also desirable cosmologically, since the range of the symmetron force grows with M . In particular, from (39), $\mu^{-1} \lesssim \text{Mpc}$ for $M \lesssim 10^{-3} M_{\text{Pl}}$.

The symmetron is observationally distinguishable from other screening mechanisms. In chameleon theory, as discussed in Sec. 2.1.2, the tightest constraint comes from laboratory tests of the inverse square law. Once this is satisfied, however, the predicted solar system deviations are unobservably small. In contrast, as mentioned above the symmetron predictions for solar system tests are just below current constraints. On the other hand, chameleon and symmetron models have in common the prediction of macroscopic violations of the WEP, which can show up in various astrophysical observations [90]. In the Vainshtein case, as mentioned in Sec. 2.3.2, the DGP model predicts modifications to the Moon's orbit that are within reach of next generation Lunar Laser Ranging observations, but light-deflection and time-delay signals are negligible.

2.3. Theories of Massive/Resonance Gravity

A class of infrared modified theories that has spurred a lot of activity involves giving the graviton a small mass or width. This is alluring from a purely theoretical perspective, because of the formidable challenge devising consistent, ghost-free theories of massive gravity has proven to be. We know how to give a mass to all particles, but doing so consistently for the graviton remains an

open problem. Besides the theoretical appeal, the main motivation remains of course the cosmological constant problem. The cosmological constant is the zero-momentum component of the stress-energy tensor, hence its backreaction depends sensitively on the nature of gravity in the far infrared.

At the linearized level, all theories of massive/resonance gravity reduce effectively to scalar-tensor theories, even in the limit of vanishing mass, where the scalar is the longitudinal mode of the graviton. This is the famous van Dam-Veltman-Zakharov (vDVZ) [114] discontinuity. The resolution is the Vainshtein mechanism [53] — non-linearities in the longitudinal dominate in the vicinity of astrophysical sources, and result in its decoupling from matter. Thus GR is approximately recovered in the solar system.

2.3.1. Fierz-Pauli Gravity and Its Discontents

The perennial challenge for theories of massive/resonance gravity is the avoidance of ghost instabilities. A theory of a single, Lorentz-invariant massive graviton [115] is generically plagued with ghosts. (The story is different for Lorentz-violating massive gravity [116, 117, 118]; for simplicity, we focus here on Lorentz-invariant mass terms.) At the linearized level, the Fierz-Pauli tensor structure [115] is chosen precisely to remove the 6th polarization mode of the graviton, which would otherwise be a ghost. But since this is no symmetry to prevent this mode from being excited non-linearly, one generically finds a ghost propagating around non-trivial backgrounds. The instabilities of massive gravity were first diagnosed by Boulware and Deser [119] in the ADM formalism: integrating out the lapse function and shift vector results in a Hamiltonian that is unbounded from below. In recent developments, a realization of massive gravity using an auxiliary extra dimension [63, 64] has been argued to have positive definite Hamiltonian.

The origin of the ghost is most transparent in the Goldstone-Stückelberg language [120, 121, 122]. As in the previous subsection, the metric fluctuation $\tilde{h}_{\mu\nu} = g_{\mu\nu} - \eta_{\mu\nu}$ is completed to a gauge-invariant object $h_{\mu\nu}$ by including the Goldstone modes. Focusing on the the longitudinal or helicity-0 mode π , we have [26]

$$h_{\mu\nu} = \tilde{h}_{\mu\nu} + \eta_{\mu\nu} \frac{\pi}{M_{\text{Pl}}} + \frac{2r_c^2}{M_{\text{Pl}}} \partial_\mu \partial_\nu \pi + \frac{r_c^4}{M_{\text{Pl}}^2} \partial_\mu \partial^\gamma \pi \partial_\nu \partial_\gamma \pi, \quad (43)$$

where the $\eta_{\mu\nu}\pi/M_{\text{Pl}}$ term is introduced for convenience to diagonalize the kinetic matrix of \tilde{h} and π . (This is the linearized version of a conformal transformation to Einstein frame.) Since $h_{\mu\nu}$ is gauge-invariant, we are allowed to add $\mathcal{L}_{\text{mass}} = \sqrt{-g} g^{\mu\nu} g^{\alpha\beta} (a h_{\mu\alpha} h_{\nu\beta} + b h_{\mu\nu} h_{\alpha\beta})$ to the Einstein-Hilbert lagrangian, where a and b are constants. Substituting the decomposition (43), we risk generating a $(\square\pi)^2$ term in the action from the square of the $\partial_\mu \partial_\nu \pi$ term, which would yield a ghost at the quadratic level. But the Fierz-Pauli structure ($a = -b$) is chosen precisely to remove this dangerous term.

We can zoom in on the Goldstone sector by taking the decoupling limit [26]: $M_{\text{Pl}} \rightarrow \infty$ and $r_c \rightarrow \infty$, keeping the strong coupling scale $(r_c^{-4} M_{\text{Pl}})^{1/5}$ fixed.

The resulting action [26, 120],

$$S_{\text{FP}} = \int d^4x \left(3\pi \square \pi + \frac{r_c^4}{M_{\text{Pl}}} \square \pi [(\square \pi)^2 - (\partial_\mu \partial_\nu \pi)^2] + \frac{1}{M_{\text{Pl}}} \pi T \right), \quad (44)$$

is clearly well-defined at the quadratic level, as advocated. However, the theory has non-linear instabilities: expanding the interaction term to quadratic order in perturbations φ around a background solution $\Pi(x)$ yields higher-derivative terms of the form $\square \Pi (\square \varphi)^2$, which signals a ghost. One could hope to remove the ghost by adding suitable higher-order terms in h can remove the ghost, but [120] argued there is insufficient freedom to do so. However, these conclusions have been questioned recently by [63] in the context of auxiliary extra dimensions. Another proposal for a non-linear version of massive gravity was proposed recently in [123].

2.3.2. Dvali-Gabadadze-Porrati Gravity

The DGP model [22, 23, 24] shares many properties of massive gravity, but avoids some of its pitfalls. See [25] for a review. In this construction, our visible universe is confined to a 3-brane embedded in an empty, 4+1-dimensional space-time, where the extra dimension has infinite-volume. The hallmark of DGP gravity is the inclusion of an Einstein-Hilbert term on the brane. The action, given by

$$S = \frac{M_5^3}{2} \int_{\text{bulk}} d^5x \sqrt{-g_5} R_5 + \frac{M_{\text{Pl}}^2}{2} \int_{\text{brane}} d^4x \sqrt{-g_4} (R_4 + \mathcal{L}_{\text{matter}}), \quad (45)$$

therefore involves two Planck scale, M_{Pl} and M_5 . The R_4 term on the brane gives a large inertia to the graviton and leads to a recovery of a $1/r^2$ force law at short distances. But since the extra dimension is infinite in extent, GR is not recovered in the infrared — instead the gravitational force law asymptotes to $1/r^3$ at large distances, corresponding to 5D gravity. The cross-over scale r_c from $1/r^2$ to $1/r^3$ is set by the bulk and brane Planck scales:

$$r_c = \frac{M_{\text{Pl}}^2}{M_5^3}. \quad (46)$$

Hence a large hierarchy between M_5 and M_{Pl} is necessary to recover the inverse-square law on sufficiently large distances. Setting $r_c \sim H_0^{-1}$, for instance, requires $M_5 \sim 100$ MeV.

From the point of view of a brane observer, the 5 helicity states of the massless 5D graviton combine to form a massive spin-2 representation in 4D. In the weak-field limit, the metric fluctuation on the brane for a given an energy-momentum source is [22, 124]

$$h_{\mu\nu} = \frac{M_{\text{Pl}}^{-2}}{-\square + r_c^{-1} \sqrt{-\square}} \left(T_{\mu\nu} - \frac{1}{3} \eta_{\mu\nu} T \right). \quad (47)$$

The infrared modification is manifest in the form of the propagator, $1/(-\square + r_c^{-1} \sqrt{-\square})$, which describes a resonance graviton with tiny width r_c^{-1} . (In the

parametrization of (69), this corresponds to $\alpha = 1/2$.) As in massive gravity, the tensor structure of the above amplitude is different than predicted by General Relativity, even in the limit $r_c \rightarrow \infty$. This is the famous vDVZ discontinuity [114] of massive gravity. As we will review shortly, this discrepancy is an artifact of perturbation theory — non-linear effects in the helicity-0 mode near astrophysical sources lead to a recovery of General Relativity. This effect, first conjectured by Vainshtein in the context of massive gravity [53, 54, 55], has been shown explicitly in DGP [125, 126, 127, 128].

Since the brane is a codimension-one object, the standard Israel junction conditions lead to a Friedmann equation which is *local* on the brane [129]:

$$H^2 = \frac{\rho}{3M_{\text{Pl}}^2} \pm \frac{H}{r_c}, \quad (48)$$

where the \pm branches correspond to different brane embeddings in the Minkowski bulk space-time. The “+” branch has generated a lot of interest because it leads to cosmic acceleration at late times without vacuum energy [129, 130]. However, it has been established that this branch of solutions suffers from ghost instabilities, first using perturbative arguments [27, 28, 131] and, more recently, by studying non-linear solutions [132, 133, 134, 135]. The “−” branch, however, is stable. (To account for cosmic acceleration, the − branch requires a vacuum energy component. Together with the H/r_c correction in (48), this leads to an effective dark energy component with $w < -1$ [136].) This is a generic property in DGP: solutions come in pairs, with one member being continuously connected to the trivial solution and having stable perturbations, while the other being connected to the self-accelerated cosmological solution and having unstable perturbations.

As in massive gravity, we can zoom in on the helicity-0 sector via a decoupling limit [27, 54]: $M_{\text{Pl}} \rightarrow \infty$ and $r_c \rightarrow \infty$, keeping the strong coupling scale $(r_c^{-2} M_{\text{Pl}})^{1/3}$ fixed. (See [137] for an argument against the validity of taking a decoupling limit in the DGP case.) In this limit, the theory becomes local on the brane and describes a scalar field π :

$$S_{\text{DGP}} = \int d^4x \left(3\pi \square \pi - \frac{r_c^2}{M_{\text{Pl}}} (\partial\pi)^2 \square \pi + \frac{1}{M_{\text{Pl}}} \pi T \right). \quad (49)$$

This theory enjoys a Galilean shift symmetry [27, 28],

$$\partial_\mu \pi \rightarrow \partial_\mu \pi + c_\mu, \quad (50)$$

which is a vestige of the full $5D$ Lorentz transformations [138]. Thus, π has been dubbed a galileon field [66, 67, 68, 69, 70, 71, 72]. Even though (49) contains higher-derivative interactions, the resulting equation of motion for π ,

$$\partial^\mu (6M_{\text{Pl}} \partial_\mu \pi + 2r_c^2 \partial_\mu \pi \square \pi - r_c^2 \partial_\mu (\partial\pi)^2) = -T, \quad (51)$$

is nevertheless second-order — all higher-derivative terms cancel out when performing the variation. This is unlike the case of massive gravity, where the variation of (44) yields a higher-order equation of motion. The π -action (51)

was generalized in [66] to include higher-derivative interactions that preserve the Galilean shift symmetry and yield second-order equations of motion.

The πT coupling generates a scalar contribution to the graviton exchange amplitude, which is responsible for the discrepancy between the $1/3$ coefficient in (47) and the expected factor of $1/2$ for a massless spin-2 field. As mentioned earlier, this discrepancy persists even as $r_c \rightarrow \infty$. In the presence of a large source, however, the self-interactions terms are important and result in the decoupling of π from the source. This Vainshtein screening can be immediately understood from (51) by considering the static, spherically-symmetric galileon profile due to a point source. With trivial asymptotic conditions, (51) can be integrated to give

$$\frac{d\pi}{dr} = \frac{3M_{\text{Pl}}r}{4r_c^2} \left(-1 + \sqrt{1 + \frac{4}{9} \frac{r_\star^3}{r^3}} \right), \quad (52)$$

where we have introduced the r_\star scale,

$$r_\star = (r_c^2 r_{\text{Sch}})^{1/3}, \quad (53)$$

with r_{Sch} denoting the Schwarzschild radius of the source. At short distances, $r \ll r_\star$, the galileon-mediated force is manifestly suppressed compared to the gravity:

$$\left. \frac{F_\pi}{F_{\text{grav}}} \right|_{r \ll r_\star} = \frac{|\vec{\nabla}\pi|}{M_{\text{Pl}}|\vec{\nabla}\Phi|} = \left(\frac{r}{r_\star} \right)^{3/2} \ll 1. \quad (54)$$

Thus, as advocated, the strong interactions of π lead to its decoupling near a source, and the theory reduces to Newtonian gravity. The deviation from standard gravity, albeit small in the solar system, is nevertheless constrained by Lunar Laser Ranging observations: $r_c \gtrsim 120$ Mpc [139, 122, 140]. A comparable bound on r_c has also been obtained by studying the effect on planetary orbits [141]. The next generation Apache Point Observatory Lunar Laser-ranging Operation will improve this bound by an order of magnitude [142], thereby probing the interesting regime $r_c \sim H_0^{-1}$.

At large distances, $r \gg r_\star$, on the other hand, the non-linear terms in π are negligible, and the resulting correction to Newtonian gravity is of order unity:

$$\left. \frac{F_\pi}{F_{\text{grav}}} \right|_{r \gg r_\star} = \frac{1}{3}. \quad (55)$$

The galileon-mediated force therefore leads to an enhancement of the gravitational attraction by a factor of $4/3$. In this far-field regime, the theory reduces to a Brans-Dicke theory with $\omega_{\text{BD}} = 0$, consistent with (47).

Unlike chameleon theories, there are no macroscopic violations of the WEP in this theory [90]. This is because (51) takes the form of a total divergence $\partial j_\pi^\mu = -T$, which follows from the shift symmetry (50). This implies a generalized ‘‘Gauss’ law’’ [28, 90]: spherically-symmetric exterior solutions for π only depend on the mass enclosed, as can be seen from (52).

The Vainshtein screening can also be understood by studying perturbations φ around a background Π profile: $\pi = \Pi + \varphi$. Expanding (49) to quadratic order in φ gives

$$S_{\text{pert}} = - \int d^4x (3\eta_{\mu\nu} + 2K_{\mu\nu} - 2\eta_{\mu\nu}K) \partial^\mu \varphi \partial^\nu \varphi, \quad (56)$$

where $K_{\mu\nu} = -r_c^2 \partial_\mu \partial_\nu \Pi / M_{\text{Pl}}$ is the extrinsic curvature of the brane in the decoupling limit. In the non-linear regime, $K \gg 1$, galileon perturbations therefore acquire a large kinetic term and decouple from matter.

We note in passing that evaluating the above kinetic matrix for the spherically-symmetric background (52) shows that perturbations propagate superluminally in the radial direction in the range $r_{\text{Sch}} \ll r \ll r_*$ [138]. Superluminal propagation is a generic property of galileon theories [66] and has recently been shown to hold around exact solutions of DGP [143]. The existence of superluminality in these models casts doubts on whether they can be completed in a quantum field theory or perturbative string theory [138].

As the above discussion illustrates, much of the DGP phenomenology (and its predictions for tests of gravity) is captured by the decoupling theory. This motivated the authors to [68] to propose a $4D$ theory of modified gravity, by promoting (49) into a fully covariant, non-linear theory of gravity coupled to a galileon field. See also [67] for covariantizations of more general galileon theories. While the extension is by no means unique, a canonical choice is

$$S = \int d^4x \sqrt{-g} \left(\frac{M_{\text{Pl}}^2}{2} e^{-2\pi/M_{\text{Pl}}} R - \frac{r_c^2}{M_{\text{Pl}}} (\partial\pi)^2 \square\pi + \mathcal{L}_{\text{matter}}[g] \right). \quad (57)$$

(The $\pi \square \pi$ term in (49) arises by diagonalizing the kinetic matrix as in (43), which also generates the πT coupling.) Remarkably, the $4D$ cosmology that follows from this action reproduces many features of the full-fledged DGP model [68]. The Friedmann equation has two branches of solutions, with stable or unstable perturbations, depending on the sign of $\dot{\pi}$. Moreover, there is a cosmological analogue of the Vainshtein effect: at early times, when the density of the universe is high, non-linear interactions in π are important, resulting in the galileon energy density being subdominant compared to the matter or radiation fluid.

2.3.3. Degravitation

One of the underlying motivations for massive/resonance gravity is the cosmological constant problem. This is usually stated as “Why is the vacuum energy so small?” But since the only observable effect of the cosmological constant is through its backreaction on the expansion of the universe, a more conservative question is “Why does the vacuum energy gravitate so weakly?” If gravity acts as a high-pass filter, in particular, a large cosmological constant can result in a small expansion rate [144, 145, 122]. The vacuum energy can thus *degravitate*. As we will see below, degravitation is closely tied to massive gravity — any theory that exhibits degravitation must reduce, at the linearized level, to a theory of massive/resonance gravity [122]. Degravitation is the gravitational analogue

to the well-known screening of charges in a superconducting (or Higgs) phase of electromagnetism [122].

A phenomenological modification to Einstein's equations that encapsulates degravitation is

$$G_N^{-1}(\square r_c^2)G_{\mu\nu} = 8\pi T_{\mu\nu}, \quad (58)$$

where Newton's constant, $G_N(\square r_c^2)$, has been promoted to a high-pass filter with cut-off scale r_c : sources with characteristic wavelength $\ll r_c$ gravitate normally, but those with wavelength $\gg r_c$ are degravitated.

Equation (58) manifestly violates the Bianchi identity — an immediate consequence of general covariance —, and hence cannot be the whole story. But there is already a problem at the linearized level, $g_{\mu\nu} = \eta_{\mu\nu} + \tilde{h}_{\mu\nu}$, where the Bianchi identity is trivially satisfied. Rewriting the filter function as $G_N^{-1}(\square r_c^2) \equiv 1 - m^2(\square r_c^2)/\square$ and choosing de Donder gauge, $\partial^\mu \tilde{h}_{\mu\nu} = \partial_\nu \tilde{h}/2$, (58) reduces to

$$(\square - m^2(\square r_c^2)) \left(\tilde{h}_{\mu\nu} - \frac{1}{2}\eta_{\mu\nu}\tilde{h} \right) = 8\pi T_{\mu\nu}. \quad (59)$$

Suppose for a moment that $m^2(\square r_c^2) \equiv m^2$ is constant. Then the problem is obvious: the only allowed (Lorentz-invariant) tensor structure of a spin-2 mass term that is ghost-free is the Fierz-Pauli form [115]: $m^2(h_{\mu\nu} - h\eta_{\mu\nu})$. The mass term in (59) is manifestly not in this form, hence it cannot describe a consistent theory of a massive spin-2 particle. Allowing for more general $m^2(\square r_c^2)$ only exacerbates things, for we can spectrally represent the graviton propagator,

$$\frac{1}{\square - m^2(\square r_c^2)} = \int_0^\infty dM^2 \frac{\rho(M^2 r_c^2)}{\square - M^2}, \quad (60)$$

and apply the argument to each massive graviton in the continuum.

The resolution of this paradox is simple: a massive graviton has 5 polarization states (2 helicity-2, 2 helicity-1 and 1 helicity-0 states), but (59) is an effective equation that only describes the helicity-2 part of the graviton, obtained by integrating out the other 3 polarization degrees of freedom. For completeness, let us briefly review the proof of [122, 146]. The starting point is a generalization of Fierz-Pauli theory [115], allowing for a momentum-dependent graviton mass:

$$(\mathcal{E}h)_{\mu\nu} + \frac{m^2(\square r_c^2)}{2}(h_{\mu\nu} - \eta_{\mu\nu}h) = 8\pi T_{\mu\nu}, \quad (61)$$

where $(\mathcal{E}h)_{\mu\nu} = -\square h_{\mu\nu}/2 + \dots$ is the linearized Einstein tensor. The diffeomorphism gauge symmetry can be made explicit by introducing a Stückelberg field A_μ [26]

$$h_{\mu\nu} = \hat{h}_{\mu\nu} + \partial_\mu A_\nu + \partial_\nu A_\mu, \quad (62)$$

such that $\delta \hat{h}_{\mu\nu} = \partial_\mu \xi_\nu + \partial_\nu \xi_\mu$ and $\delta A_\mu = -\xi_\mu$ under gauge transformations. Thus $h_{\mu\nu}$ is gauge invariant. This is analogous to electromagnetism in a Higgs (or superconducting) phase in which the photon becomes a gauge-invariant observable: $A_\mu = \tilde{A}_\mu + \partial_\mu \phi$.

The idea is to solve for A_μ and substitute the result back into (61) to obtain an equation for the helicity-2 modes. First, we substitute the decomposition (62) into (61):

$$(\mathcal{E}\hat{h})_{\mu\nu} + m^2(\square r_c^2) \left(\hat{h}_{\mu\nu} - \eta_{\mu\nu}\hat{h} + \partial_\mu A_\nu + \partial_\nu A_\mu - 2\eta_{\mu\nu}\partial^\alpha A_\alpha \right) = 8\pi T_{\mu\nu}. \quad (63)$$

Taking the divergence of this expression allows us to isolate an equation for A_μ :

$$\partial^\mu F_{\mu\nu} = -\partial^\mu \left(\hat{h}_{\mu\nu} - \eta_{\mu\nu}\hat{h} \right), \quad (64)$$

where $F_{\mu\nu} \equiv \partial_\mu A_\nu - \partial_\nu A_\mu$. Note that taking another divergence yields: $\partial^\mu \partial^\nu \hat{h}_{\mu\nu} - \square \hat{h} = 0$, hence \hat{h} can be represented in the form $\hat{h}_{\mu\nu} = \tilde{h}_{\mu\nu} - \eta_{\mu\nu} \Pi_{\alpha\beta} \tilde{h}^{\alpha\beta} / 3$, where $\Pi_{\alpha\beta} = \eta_{\alpha\beta} - \partial_\alpha \partial_\beta / \square$ is the transverse projector. Thus $\tilde{h}_{\mu\nu}$ carries two degrees of freedom. Coming back to (64), the solution for A_μ is

$$A_\nu = -\frac{1}{\square} \partial^\mu \left(\hat{h}_{\mu\nu} - \eta_{\mu\nu}\hat{h} \right) - \partial_\nu \Theta, \quad (65)$$

where Θ is an arbitrary gauge function. Substituting (65) back into (63), and choosing Θ appropriately, we find

$$\left(1 - \frac{m^2(\square r_c^2)}{\square} \right) (\mathcal{E}\tilde{h})_{\mu\nu} = 8\pi T_{\mu\nu}, \quad (66)$$

which is the linearized version of (58). Therefore, as advocated, (59) is an effective equation for the helicity-2 part $\tilde{h}_{\mu\nu}$, after integrating out the extra helicities of a massive spin-2 representation.

Hence, any theory that proposes to filter out the cosmological constant must reduce, in the weak-field limit, to a theory of massive or resonance gravity. Of course the reverse is not true — not every theory of massive/resonance gravity will exhibit degravitation at the non-linear level. To see degravitation at work at the linearized level, consider (61) for vacuum energy, $T_{\mu\nu} = -\Lambda \eta_{\mu\nu}$, and let us focus on the case of constant m^2 for simplicity:

$$(\mathcal{E}h)_{\mu\nu} + \frac{1}{2r_c^2} (h_{\mu\nu} - \eta_{\mu\nu}h) = -8\pi \Lambda \eta_{\mu\nu}. \quad (67)$$

Note that without the mass term the solution grows unbounded, $h_{ij} \sim \Lambda(t^2 \delta_{ij} + x_i x_j) / 6$, which is the weak-field version of de Sitter space. With the mass term turned on, however, the solution is just flat space

$$h_{\mu\nu} = \frac{\Lambda r_c^2}{3} \eta_{\mu\nu}. \quad (68)$$

Thus the gravitational backreaction of Λ vanishes in a theory of a massive spin-2 particle.

What functional forms for $m^2(\square r_c^2)$ are allowed? A useful parametrization is the power-law form [122, 146]

$$m^2(\square r_c^2) = r_c^{-2(1-\alpha)} (-\square)^\alpha, \quad (69)$$

where α is a constant. First, in order for the modification to be relevant in the infrared, we must impose $\alpha < 1$, otherwise the mass term becomes negligible as $\square \rightarrow 0$. Second, in order for the graviton propagator to have a positive definite spectral density, $\rho(M^2) \geq 0$ in (60), we must require $\alpha \geq 0$. Otherwise the left-hand side of (60) vanishes as $\square \rightarrow 0$, which is inconsistent with $\rho(M^2) \geq 0$. Finally, in [122] it was argued that $\alpha < 1/2$ is necessary in order for the degravitation phenomenon to be effective in a certain decoupling limit of the theory. Hence, the allowed range is

$$0 \leq \alpha < \frac{1}{2}. \quad (70)$$

The lower bound corresponds to a hard mass for the graviton, discussed in Sec. 2.3.1. The range $\alpha > 0$ corresponds to a continuum of massive graviton states, which immediately points to extra dimensions of infinite extent. The best known example is the DGP model (Sec. 2.3.2), with $D = 5$ bulk space-time dimensions. The DGP mass term, $m^2(\square r_c^2) = r_c^{-1} \sqrt{-\square}$, corresponds to $\alpha = 1/2$, which coincides with the upper bound of (70). Cascading gravity theories (Sec. 2.3.4) generalize the DGP scenario to higher dimensions. As we will see in Sec. 2.3.4, all such theories correspond to $\alpha \approx 0$ in the far infrared.

2.3.4. Cascading Gravity

It is natural to ask how the DGP model extends to higher dimensions. Purely from a phenomenological perspective, it is certainly worthwhile to explore this wider class of infrared modifications to gravity. A second motivation, however, is the degravitation approach to the cosmological constant problem. The standard DGP model fails to exhibit degravitation. Although the DGP propagator is of the desired form for degravitating the cosmological constant, unfortunately (48) does not exhibit degravitation — a large brane tension generates rapid Hubble expansion on the brane. This is consistent with the degravitation condition (70), which requires $\alpha < 1/2$.

On the other hand, theories with $D > 6$ bulk space-time dimensions all correspond to $\alpha \approx 0$ in the far infrared [59]. Since gravity is D -dimensional in the infrared, the gravitational potential scales as $1/r^{D-3}$ in this limit. Expanding in terms of massive states,

$$\Phi(r) = \int_0^\infty dM^2 \rho(M^2) \frac{e^{-Mr}}{r} \sim \frac{1}{r^{D-3}}, \quad (71)$$

the spectral density must satisfy $\rho(M^2) \sim M^{D-6}$ as $M \rightarrow 0$. Therefore, in the small momentum limit ($\square \rightarrow 0$),

$$\lim_{\square \rightarrow 0} \frac{1}{\square - m^2(\square r_c^2)} \sim \int_0^\infty dM^2 \frac{M^{D-6}}{M^2}. \quad (72)$$

The integral converges for $D > 6$. Therefore, all such theories correspond to $\alpha = 0$ in the infrared. For $D = 6$, the integral is logarithmically divergent, corresponding to $m^2(\square r_c^2) \sim \log \square$.

Realizing these higher-dimensional scenarios has been notoriously difficult. To begin with, the simplest constructions are plagued by ghost instabilities, even around a flat space background [147, 148]. Secondly, because of the higher-codimension nature of the brane, the $4D$ propagator is divergent and must be regularized [151, 152, 153], usually by giving the brane a finite thickness. Finally, for a static bulk, the geometry for codimension $N > 2$ has a naked singularity at finite distance from the brane, for arbitrarily small tension [144]. (Interestingly, however, it has been argued that allowing the brane to inflate results in a Hubble rate on the brane which is *inversely* proportional to the brane tension for codimension $N > 2$ [144].)

Recently, it was argued that these pathologies are resolved by embedding our 3-brane within a succession of higher-dimensional branes, each with their own induced gravity term, embedded in one another in a flat D -dimensional bulk [58, 59, 60]. See [154] for a pedagogical review. In the simplest codimension-2 case, our 3-brane is embedded in a 4-brane within a flat $6D$ bulk, with action

$$\begin{aligned}
S &= \frac{M_6^4}{2} \int_{\text{bulk}} d^6 x \sqrt{-g_6} R_6 + \frac{M_5^3}{2} \int_{4\text{-brane}} d^5 x \sqrt{-g_5} R_5 \\
&+ \frac{M_{\text{Pl}}^2}{2} \int_{3\text{-brane}} d^4 x \sqrt{-g_4} (R_4 + \mathcal{L}_{\text{matter}}) .
\end{aligned} \tag{73}$$

The gravitational force law therefore “cascades” from $4D$ ($1/r^2$) to $5D$ ($1/r^3$) to $6D$ ($1/r^4$) etc., as we probe larger distances on the 3-brane, with the cross-over scales set by the ratios $m_5 = M_5^3/M_{\text{Pl}}^2$ and $m_6 = M_6^4/M_5^3$. A similar cascading behavior of the force law was also obtained recently in a different codimension-two framework [155]. Closely related work on intersecting branes was discussed in [156] with somewhat different motivations. See [65, 140, 157, 158] for cosmological explorations, and [159] for self-accelerated solutions in this context.

As claimed, the induced (scalar) propagator on the 3-brane is completely regular [58, 59]:

$$\mathcal{G}(p) \sim \frac{1}{p^2 + m_5 g(p^2)} , \tag{74}$$

where

$$g(p^2) = \begin{cases} \frac{\pi}{4} \frac{\sqrt{m_6^2 - p^2}}{\tanh^{-1}\left(\sqrt{\frac{m_6 - p}{m_6 + p}}\right)} & \text{for } p < m_6 \\ \frac{\pi}{4} \frac{\sqrt{p^2 - m_6}}{\tan^{-1}\left(\sqrt{\frac{p - m_6}{p + m_6}}\right)} & \text{for } p > m_6 . \end{cases} \tag{75}$$

If $m_5 > m_6$, then the Fourier transform of (74) for a point source yields a potential that cascades from $1/r$ (for $r \ll r_5$) to $1/r^2$ (for $m_5^{-1} \ll r \ll m_6^{-1}$) to $1/r^3$ (for $r \gg m_6^{-1}$). Note the crucial role played by the 4-brane: in the limit $M_5 \rightarrow 0$, one recovers the logarithmic divergence, $\mathcal{G}(p) \sim \log p$, characteristic of codimension-2 branes [151]. This can be understood intuitively as follows. Because of the $5D$ Einstein-Hilbert term, the force law must become approximately $5D$ at short distances on the 4-brane. Hence the lower-dimensional

brane behaves effectively as a codimension-1 source, whose Green's function is therefore regular. These conclusions straightforwardly generalize to arbitrary D dimensions.

The ghost issue is trickier. Perturbing around the flat space solution with empty branes, one finds that a ghost scalar mode propagates. In the 6D case, this is seen most directly from the tensor structure of the one-graviton exchange amplitude between conserved sources on the 3-brane in the UV limit [58, 59]:

$$\mathcal{A} \sim T^{\mu\nu} \cdot \frac{1}{\square} \cdot \left(T'_{\mu\nu} - \frac{1}{3} \eta_{\mu\nu} T' \right) - \frac{1}{6} T \cdot \frac{1}{\square} T'. \quad (76)$$

We have conveniently separated terms as the sum of a massive spin-2 contribution, with the well-known $1/3$ coefficient, plus a contribution from a conformally-coupled scalar. The problem is with this scalar mode. The last term in (76) is negative, indicating a ghost mode. This UV behavior is identical to other higher-dimensional scenarios [147, 148].

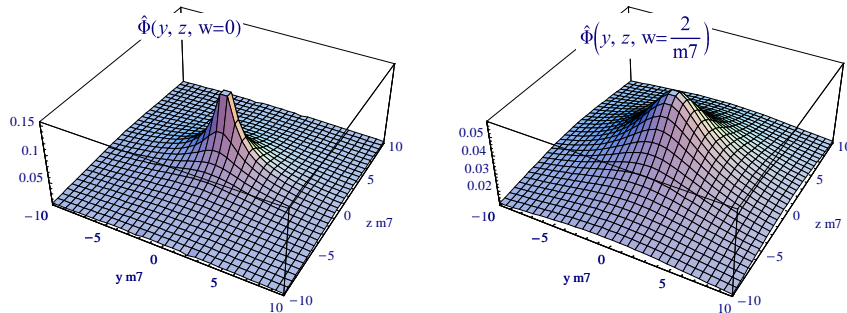


Figure 2: Plot of the $D = 7$ cascading solution for the gravitational potential $\hat{\Phi}(y, z, w)$ resulting from a small tension on the codimension-3 brane. The solution is shown for $w = 0$ and $w = 2m_7^{-1}$ in the case where $m_6 = m_7$. In terms of the extra-dimensional coordinates y, z and w , the codimension-1 brane is located at $w = 0$, the codimension-2 brane at $z = w = 0$, and the codimension-3 brane at $y = z = w = 0$.

However it was immediately noticed [58] that the ghost is removed by adding a sufficiently large tension Λ on the 3-brane. (Alternatively, the ghost is also cured when considering a higher-dimensional Einstein-Hilbert term localized on the brane [148, 149, 59].) In analogy with a cosmic string in ordinary $4D$ gravity, adding tension to a codimension-2 defect leaves the induced geometry flat but creates a deficit angle. The exchange amplitude in this case becomes [58, 62]

$$\mathcal{A} \sim T^{\mu\nu} \cdot \frac{1}{\square} \cdot \left(T'_{\mu\nu} - \frac{1}{3} \eta_{\mu\nu} T' \right) + \frac{1}{6 \left(\frac{3\Lambda}{2m_6^2 M_{\text{Pl}}^2} - 1 \right)} T \cdot \frac{1}{\square} T'. \quad (77)$$

The scalar contribution is therefore healthy provided that

$$\Lambda \geq \frac{2}{3} m_6^2 M_{\text{Pl}}^2. \quad (78)$$

Note again the essential role played by the 4-brane kinetic term: in the limit $M_5 \rightarrow 0$ (keeping M_{Pl} and M_6 fixed), we have $m_6 \rightarrow \infty$, and hence (78) cannot be satisfied. A limitation of the original derivation of (78) is that it was derived in a decoupling limit of (73). Recently, this result was confirmed by perturbing the full $6D$ action (73) around a background including tension on the 3-brane [62]. The background geometry is flat everywhere, but the extra dimensions show a deficit angle due to the codimension-2 source. (Just as in DGP, the helicity-0 and conformally-coupled scalar modes contributing to (77) should decouple non-linearly due to the Vainshtein screening effect.)

The $D = 6$ framework already exhibits degravitation: as mentioned above, a 3-brane with tension creates a deficit angle in the bulk while remaining flat. This self-tuning mechanism crucially relies on the extra dimensions having infinite volume: if the dimensions were compact, the brane tension would have to be tuned against other branes and/or bulk fluxes [160]. Since the deficit angle must be less than 2π , however, the tension allowed by the solutions considered in [58, 62] is bounded

$$\Lambda < 2\pi M_6^4, \quad (79)$$

where the $6D$ Planck mass is itself constrained phenomenologically, $M_6 \sim \text{meV}$. Given the geometrical origin of this bound, it is most likely an artifact of the codimension-2 case and is expected to be absent in higher-codimension.

Motivated by these considerations, [61] considered the case of $D = 7$ Cascading Gravity, consisting of a 3-brane living on a 4-brane, itself embedded in a 5-brane, together in a 6+1-dimensional bulk. Including tension on the 3-brane, these authors derived a solution for which the induced 3-brane geometry is exactly flat. The hope is that in this case brane tension can still degravitate without being limited by a bound analogous to (79). Unlike the case of a pure codimension-3 DGP brane in 6+1 dimensions, where the static bulk geometry has a naked singularity for arbitrarily small tension [144], here the bulk metric is non-singular everywhere (except, of course, for a delta-function in curvature at the 3-brane location) and asymptotically flat. This smoothness of the solution traces back to the cascading mechanism of regulating the propagator: the presence of parent branes removes the power-law divergence in the $4D$ propagator.

Figure 2 shows the gravitational potential as a function of the 3 extra-dimensional coordinates, y, z and w , with the codimension-1 brane located at $w = 0$, the codimension-2 brane at $z = w = 0$, and the codimension-3 brane at $y = z = w = 0$. Here, $m_7 = M_7^5/M_6^4$ denotes the cross-over scale from $6D$ to $7D$. Thanks to the cascading mechanism, which has regularized all potential divergences, the solution shown in Fig. 2 is finite everywhere. Because the metric depends on 3 spatial coordinates, the analytical results of [61] was restricted to the weak-field approximation, corresponding to sufficiently small tension. Ongoing numerical work is aimed at extending these solutions to the non-linear regime of large tension [161].

3. Tests from Astronomical Observations

The most stringent current tests of gravity come from laboratory and solar system tests, spanning millimeter to AU scales. In addition, the production of gravity waves predicted by GR is tested by binary pulsar observations. These tests are summarized above in Sec. 1 and described in Will’s review [1].

Astrophysical probes of gravity on kpc–Mpc scales include galaxy rotation curves, satellite dynamics and other dynamical and lensing properties of galaxies and clusters. On scales of 1 Mpc to over 1 Gpc, tests using the large-scale structure in the universe are being devised using the distribution of galaxies, dark matter (via lensing) and cross-correlations with the CMB. These astrophysical/cosmological tests are the subject of this section.

Modifications in gravity can also affect the propagation of gravitational waves. Future gravitational wave experiments such as LISA can detect gravitational waves from distant supermassive black hole pairs in the coalescence phase [162]; however these tests as well as a variety of other tests of gravity in the strong field regime are beyond the scope of this review.

3.1. Early Universe Tests

The two observational probes of the early universe are Big Bang Nucleosynthesis (BBN) when the universe was $\sim 10 - 100$ seconds old and the Cosmic Microwave Background (CMB) which last scattered when the universe was $\sim 400,000$ years old. The abundance of light elements, in particular Helium and Deuterium, produced during BBN is very sensitive to the expansion rate H of the universe and the temperature and time elapsed between the freeze out of neutrons and protons and BBN (see [163] for a review). Its sensitivity to H and T means that the light element abundance tests the Friedmann equation, which can be written as: $H^2 \sim Gg_*T^4$, assuming radiation domination and neglecting spatial curvature. Given our knowledge of g_* , the number of relativistic species at BBN, this test is usually stated as a constraint on the deviation of the Gravitational constant G from Newton’s value G_N . Current constraints on G are somewhat better than 10%. The value and constraints on G are quite sensitive to our knowledge of g_* (and generally assume the current values for non-gravitational constants such as the fine structure constant).

The CMB at the epoch of last scattering, $z \simeq 1100$, does not yet offer as clean a test of the Friedmann equation as BBN. The reason is that there is a significant degeneracy between G and H unless precise information on the CMB anisotropy power spectrum is available [164]. A higher value of G leads to a delay in the epoch of recombination thus causing greater damping of the CMB power spectrum at high angular wavenumber ℓ . Using present data on the CMB temperature anisotropy power spectrum from the WMAP measurement plus smaller scale data [165] obtain constraints on G at nearly the 10% level. Combining the constraint with BBN, assuming a constant G between BBN and $z \simeq 1100$, improves constraints by a factor of 3. The CMB constraint is limited by the fact that other parameters, in particular the spectral index of

the primordial power spectrum, can mimic the change in the damping due to deviations in G .

With the expected measurement of the polarization power spectrum from the PLANCK satellite, this degeneracy gets broken and the CMB constraints approach the level of 1% [165]. Thus with PLANCK and future cosmic variance limited measurements of the CMB polarization the constraints on G approach the level of current laboratory measurements.

3.2. Large-Scale Structure Tests

Structure formation in modified gravity in general differs [166, 167, 168, 169, 170, 171, 172, 173, 174, 175, 176, 177, 178, 140, 157, 158] from that in GR. Perturbative calculations at large scales have shown that it is promising to connect predictions in these theories with observations of large-scale structure (LSS). On small scales even larger deviations may occur around galaxy and cluster halos, depending on how the theory transitions to GR. Nevertheless, carrying out robust tests of MG in practice is challenging. The two approaches that have been taken are to either constrain the parameters of a particular model by working out its predictions for the growth of structure, or to define effective parameters in the spirit of the PPN formalism used to test GR in the solar system. While both approaches have their limitations, we shall see below that there has been recent progress and upcoming surveys offer great promise for tests of gravity.

There are three regimes for the growth of perturbations: the superhorizon regime, the quasi-static Newtonian regime of linear growth, and the small scale, nonlinear regime. The quasi-static Newtonian regime is valid for non-relativistic motions and length scales sufficiently smaller than the horizon. In this regime (discussed in the next sub-section) the linearized fluid equations in expanding coordinates are sufficient to describe perturbations. In the nonlinear regime, while gravity is still in the weak field limit, density fluctuations are no longer small and in addition the density/potential fields may couple to additional scalar fields introduced in MG theories. The nonlinear regime is therefore the hardest to describe in any general way as the nature of the coupling to scalar fields is theory specific. It may well be the most discriminatory for some theories as there can be a rich phenomenology ranging from galaxy cluster to solar system and laboratory scales.

3.2.1. Metric and fluid perturbations

In the Newtonian gauge, scalar perturbations to the metric are fully specified by two scalar potentials Ψ and Φ :

$$ds^2 = -(1 + 2\Psi) dt^2 + (1 - 2\Phi) a^2(t) d\vec{x}^2, \quad (80)$$

where $a(t)$ is the expansion scale factor. This form for the perturbed metric is fully general for any metric theory of gravity, aside from having excluded vector and tensor perturbations (see [179] and references therein for justifications). Note that Ψ corresponds to the Newtonian potential for the acceleration of

particles, and that in General Relativity $\Phi = \Psi$ in the absence of anisotropic stresses.

A metric theory of gravity relates the two potentials above to the perturbed energy-momentum tensor. We introduce variables to characterize the density and velocity perturbations for a fluid, which we will use to describe matter and dark energy (we will also consider pressure and anisotropic stress below). The density fluctuation δ is given by

$$\delta(\vec{x}, t) \equiv \frac{\rho(\vec{x}, t) - \bar{\rho}(t)}{\bar{\rho}(t)}, \quad (81)$$

where $\rho(\vec{x}, t)$ is the density and $\bar{\rho}(t)$ is the cosmic mean density. The second fluid variable is the divergence of the peculiar velocity

$$\theta_v \equiv \nabla_j T_0^j / (\bar{p} + \bar{\rho}) = \vec{\nabla} \cdot \vec{v}, \quad (82)$$

where \vec{v} is the (proper) peculiar velocity. Choosing θ_v instead of the vector \mathbf{v} implies that we have assumed \mathbf{v} to be irrotational. This approximation is sufficiently accurate in the linear regime for minimally coupled MG models.

In principle, observations of large-scale structure can directly measure the four perturbed variables introduced above: the two scalar potentials Ψ and Φ , and the density and velocity perturbations specified by δ and θ_v . As shown below, these variables are the key to distinguishing MG models from GR plus dark energy. Each has a scale and redshift dependence, so it is worth noting which variables and at what scale and redshift are probed by different observations. It is convenient to work with Fourier transforms, such as:

$$\hat{\delta}(\vec{k}, t) = \int d^3x \delta(\vec{x}, t) e^{-i\vec{k}\cdot\vec{x}}. \quad (83)$$

When we refer to length scale λ , it corresponds to a statistic such as the power spectrum on wavenumber $k = 2\pi/\lambda$. We will henceforth work exclusively with the Fourier space quantities and drop the $\hat{}$ symbol for convenience.

The evolution of perturbations can be calculated in the linear regime. We follow the formalism and notation of [180], except that we use physical time t instead of conformal time. We are interested in the evolution of perturbations after decoupling, so we will neglect radiation and neutrinos as sources of perturbations.

The superhorizon regime is the most constrained and simplest to describe. As pointed out by [179], any metric theory of gravity that also obeys the Einstein equivalence principle must satisfy a universal evolution equation for metric perturbations. In the conformal Newtonian gauge, for adiabatic initial conditions, this evolution is given by:

$$\ddot{\Phi} - \frac{\ddot{H}}{\dot{H}}\dot{\Phi} + H\dot{\Psi} + \left(2\dot{H} - \frac{H\ddot{H}}{\dot{H}}\right)\Psi = 0. \quad (84)$$

The above equation is equivalent to Eqn. (7) of [49] which uses a different time variable and the opposite sign for Ψ . By treating the ratio of metric potential

Φ/Ψ as a constant parameter of a MG theory, one can solve this equation for a given background solution $H(t)$. The ISW effect discussed below extends to very large scales and probes the superhorizon regime.

3.2.2. Quasi-static Newtonian Regime

In what follows, we will for the most part make the approximation of non-relativistic motions and restrict ourselves to sub-horizon length scales. One can also self-consistently neglect time derivatives of the metric potentials in comparison to spatial gradients. These approximations will be referred to as the quasi-static, Newtonian regime. Using the linearized fluid equations, the evolution of density (or velocity) perturbations can be described by a single second order differential equation:

$$\ddot{\delta} + 2H\dot{\delta} + \frac{k^2\Psi}{a^2} = 0. \quad (85)$$

With $\delta(\vec{k}, t) \simeq \delta_{\text{initial}}(\vec{k})D(k, t)$, we can substitute for Ψ in terms of δ using the Poisson equation. Here we write the Poisson equation with the sum of potentials on the left-hand side, as this is convenient for describing lensing and the ISW effect. Using the generalized gravitational “constant” \tilde{G}_{eff} we have

$$k^2(\Psi + \Phi) = -8\pi\tilde{G}_{\text{eff}}(k, t)\bar{\rho}\delta. \quad (86)$$

Using the two equations above, we obtain for the linear growth factor $D(k, t)$:

$$\ddot{D} + 2H\dot{D} - \frac{8\pi\tilde{G}_{\text{eff}}}{(1 + \Phi/\Psi)}\bar{\rho} D = 0. \quad (87)$$

From the above equation one sees readily how the combination of G_{eff} and Φ/Ψ alters the linear growth factor. Further, if these parameters have a scale dependence, then even the linear growth factor D becomes scale dependent, a feature not seen in smooth dark energy models.

We will use the power spectra of various observables to describe their scale dependent two point correlations. As an example, the 3-dimensional power spectrum of the density contrast $\delta(k, z)$ is defined as

$$\langle \delta(\vec{k}, z)\delta(\vec{k}', z) \rangle = (2\pi)^3\delta_{\text{D}}(\vec{k} + \vec{k}')P_{\delta\delta}(k, z), \quad (88)$$

where we have switched the time variable to the observable redshift z . The power spectra of perturbations in other quantities are defined analogously. We will denote the cross-spectra of two different variables with appropriate subscripts. For example, $P_{\delta\Psi}$ denotes the cross-spectrum of the density perturbation δ and the potential Ψ .

Figure 3 shows the linear and nonlinear power spectra $P_{\delta\delta}(k, z)$ for $f(R)$ and the normal branch DGP models [181]. The dotted curves show the fractional departures of the $f(R)$ linear power spectrum (left panel) and normal branch DGP (right panel) to Λ CDM. These are simply the ratio of the square of the

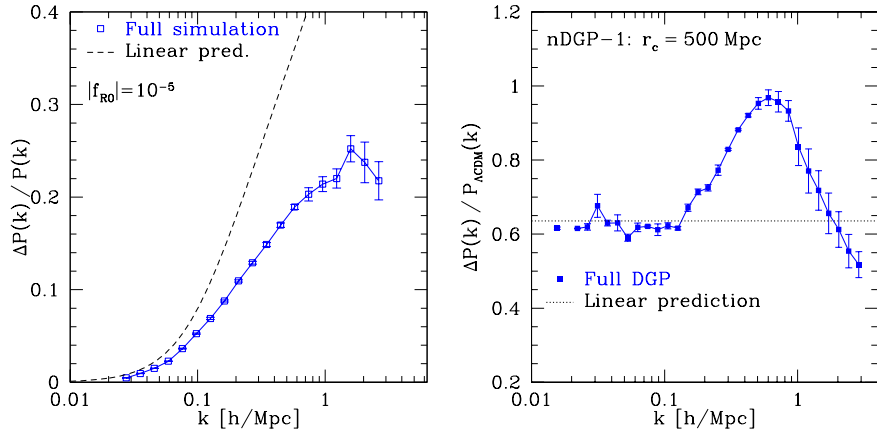


Figure 3: Power spectra for $f(R)$ (left panel) and DGP (right panel) theories. The fractional deviation from Λ -CDM are shown for the present day linear and nonlinear power spectra [181]. At high- k (small scales), nonlinear gravitational clustering and the screening of massive halos alters the power spectrum. The limited resolution of the simulations precludes a definitive statement about the high- k limit of the power spectra.

linear growth factors. The strong scale dependence is evident in the $f(R)$ case. In both cases significant deviations are evident at wavenumbers $k \gtrsim 0.1 h/\text{Mpc}$. The DGP model shown here is the normal branch, which has stronger gravitational forces than GR (the self-accelerating branch has weaker forces than GR). The nonlinear power spectra have smaller deviations from GR at high- k in part because the nonlinear contributions are similar for the MG models and Λ CDM at sufficiently high wavenumbers. The screening mechanism within massive halos is the other reason the deviations decrease at high- k , but the simulations used do not have the resolution required to fully evaluate this contribution.

It has been argued that a scale dependence in the MG parameters is generically expected for scalar-tensor theories [182]. Provided the interaction can be expressed in the Yukawa form, one expects a correction to the growth factor that is quadratic in wavenumber k . The authors of [183] have also argued that the junction condition across the brane in DGP like theories lead to a linear scale dependent term that can be significant on scales approaching the horizon.

We can also use the relations given above to obtain the linear growth factors for the velocity and the potentials from D . The growth factor for the velocity divergence is given in the following sub-section, while the Poisson equation determines the evolution of the potentials.

3.2.3. Tests using Lensing, ISW and Dynamical Observables

For tests of gravity, observables that rely directly on the change in energy or direction of photons are distinct from those that measure the clustering or dynamics of tracers such as galaxies or galaxy clusters, which have non-relativistic motions. We summarize the primary observables that provide tests of gravity

on cosmological scales in this sub-section, and consider galaxy and cluster scale tests in the following sub-section. We closely follows the treatment of Jain & Zhang [184].

The CMB power spectrum at angular wavenumber l is given by a projection along the line of sight:

$$C_{TT}(l) = \int dk \int dz F_{\text{CMB}}(k, l, z) j_l[kr(z)], \quad (89)$$

where r denotes the comoving angular diameter distance and the spherical Bessel function j_l is the geometric term through which the CMB power spectrum depends on the distance to the last scattering surface. The function F_{CMB} combines several terms describing the primordial power spectrum and the growth of the potential up to last scattering. We will regard F_{CMB} as identical to the GR prediction since we do not invoke MG in the early universe. (See Section 3.1 for a discussion of CMB constraints on G and its degeneracy with other parameters).

The ISW effect: The CMB anisotropy does receive contributions at redshifts below last scattering, in particular due to the integrated Sachs Wolfe (ISW) effect [185]. In the presence of dark energy or due to modifications in gravity, gravitational potentials evolve in time and produce a net change in the energy of CMB photons:

$$\left. \frac{\Delta T}{T} \right|_{\text{ISW}} = - \int \frac{d(\Psi + \Phi)}{dt} \frac{a(z) dz}{H(z)}. \quad (90)$$

The ISW effect, like gravitational lensing, depends on and probes the combination $\Psi + \Phi$. The ISW signal is overwhelmed by the primary CMB at all scales except for a bump it produces at the largest scales in the CMB power spectrum. For this reason, it is more effectively measured indirectly, through cross-correlation with tracers of large scale structure at low redshift. The resulting cross-correlation signal is a projection of $P_{g(\dot{\Psi} + \dot{\Phi})}(k, \chi)$, the cross-power spectrum of $(\dot{\Psi} + \dot{\Phi})$ and galaxies (or other tracers of the LSS such as quasars or clusters). By cross-correlating the CMB temperature with galaxy over-density δ_g , the ISW effect has been detected at $\lesssim 5\sigma$ confidence level [186] and provides independent evidence for dark energy, given the prior of a spatially flat universe and GR. It has also provided useful constraints on MG theories as discussed below in Section 3.3.

Gravitational Lensing: Lensing observables are the result of coherent deflections of light by mass concentrations. For the metric of Eqn. 80, the first order perturbation to a photon trajectory is given by (generalizing for example Eqn. (7.72) of [187]):

$$\frac{d^2 x^{(1)\mu}}{d\lambda^2} = -q^2 \vec{\nabla}_\perp (\Psi + \Phi). \quad (91)$$

where q is the norm of the tangent vector of the unperturbed path and $\vec{\nabla}_\perp$ is the gradient transverse to the unperturbed path. This gives the deflection angle

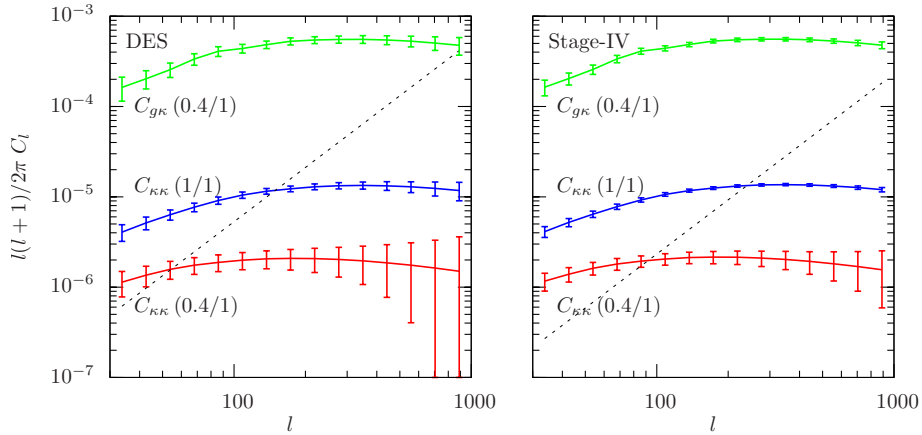


Figure 4: Examples of the shear-shear and galaxy-shear power spectra for the DES (left panel) and a Stage-IV survey similar to LSST (right panel) [190]. The upper (green) curves show the galaxy-shear cross power spectrum $C_{g\kappa}$, with foreground galaxies at $z = 0.4$ and background galaxies at $z = 1$. The lower two curves show the shear-shear power spectrum $C_{\kappa\kappa}$ with two choices of redshift bins as indicated. The error bars include the sample variance and shape noise for the two surveys (see Table 1 for survey parameters). The shape noise contribution to $C_{\kappa\kappa}$ for $z = 1$ is shown separately as well (dashed lines).

formula

$$\alpha_i = - \int \partial_i(\Psi + \Phi) ds, \quad (92)$$

where $s = q\lambda$ is the path length and α_i is the i -th component of the deflection angle (a two-component vector on the sky). Since all lensing observables are obtained by taking derivatives of the deflection angle, they necessarily depend only on the combination $\Psi + \Phi$ (to first order in the potentials). The convergence for example is given by the line-of-sight projection:

$$\kappa(\theta) = \frac{1}{2} \int_0^{z_s} \frac{dz}{H(z)} \frac{r(z)r(z_s, z)}{r(z_s)} \nabla_\theta^2(\Psi + \Phi), \quad (93)$$

We take the sources to lie at redshift z_s . The primary observables used in weak lensing are the two-point correlations of the observed shapes of galaxies and the cross-correlation of foreground galaxies with the shapes of background galaxies.

The metric potentials are related to the mass distribution by (86) so the lensing power spectra can be expressed in terms of the three-dimensional mass power spectrum $P_{\delta\delta}(k, z)$. In the small-sky-patch limit the Limber approximation [188] gives

$$C_{\kappa_i \kappa_j}(l) = \frac{9}{4} \Omega_m^2 H_0^4 \int_0^\infty \frac{dz}{H(z)a^2} \zeta^2(k, z) P_{\delta\delta}(k, z) W_L(z, z_i) W_L(z, z_j), \quad (94)$$

where the function ζ contains the modified gravity parameters: $\zeta = G/G_N[(\Phi + \Psi)/\Phi]$ expressed in Fourier space. The lensing weight function $W_L(z, z_k)$ depends on the geometry and the redshift distribution of lensed galaxies. The

three-dimensional wavenumber k is given by $k = l/r(z)$. By dividing the galaxy distribution into bins in redshift [189] a number of auto and cross-spectra can be measured. The redshift dependence of these lensing spectra carries information about the growth of structure that can test gravity theories. The galaxy-shear cross-spectrum $C_{g\kappa}$ can be defined in a similar way to $C_{\kappa\kappa}$: it is proportional to $b \Omega_m \zeta$, where b is the galaxy bias parameter. $C_{g\kappa}$ is easier to measure and can be used to test gravity as discussed below. Examples of the two lensing spectra are shown in Figure 4 for two different survey parameters [190]. Statistical errors are shown for the different power spectra – it is evident that if systematic errors can be controlled, upcoming surveys will provide percent level measurements [191].

Lensing observables probe the sum of metric potentials – this follows from the geodesic equation applied to photons and is therefore true for any metric theory of gravity. Moreover the relation of the sum of metric potentials to the mass distribution is very close to that of GR in scalar-tensor theories that we have considered [192]. Since the Einstein frame is obtained through a conformal transformation which cannot alter null geodesics, the scalar field does not directly alter the geodesics of light rays. Thus the deflection angle formula (92) and Poisson equation (86) in the form given above are essentially unaltered in these scalar-tensory gravity theories. Masses of halos inferred from lensing are the true masses. Therefore tests of gravity that rely solely on lensing measurements can only be done by using multiple source redshifts to probe the growth of structure (*e.g.*, [193]). It is more useful to combine lensing with other observations of large-scale structure.

Galaxy and cluster dynamics: MG theories do alter the force experienced by Newtonian test bodies. Thus the Newtonian potential Ψ differs from its value in GR in both DGP and $f(R)$ theories. It can be stronger by a factor of 4/3 in a certain regime in $f(R)$ gravity (on scales between those of chameleon effects and the Compton wavelength of the f_R field). This corresponds to the ratio $\Phi/\Psi = 1/2$ with the sum $\Psi + \Phi$ remaining unaltered as discussed above. Thus for a given mass distribution, significant force enhancements can occur. For DGP gravity, similar force enhancements occur for the normal branch. In particular, the dynamical masses of halos inferred from observations relying on the virial theorem or hydrostatic equilibrium can be significantly larger than the lensing (or true) masses (*e.g.*, [184, 194]). However in general the ratio of metric potentials is scale-dependent in MG theories, and force modifications can depend on halo mass and environment, so it is not straightforward to use dynamical and lensing masses to obtain Φ/Ψ .

Constraints on the Newtonian potential Ψ on small scales are obtained using dynamical probes, typically involving galaxy or cluster velocity measurements. On sub-Mpc scales, the Virial theorem for self-gravitating systems in equilibrium can be used to constrain Ψ in galaxy and cluster halos. Velocity tracers for galaxies include stars and neutral Hydrogen gas within the halos and satellite galaxies that orbit the outer parts of halos. For galaxy clusters the tracers are member galaxies and the X-ray emitting hot gas, which is also mapped using the Sunyaev Zel’dovich (SZ) effect. For relaxed clusters the hot gas is assumed

to be in hydrostatic equilibrium within the gravitational potential of the halo.

On large scales, observables depend on the linear growth factor $D(t)$ given by (85), which determines the clustering of matter and is dependent only upon the Newtonian potential Ψ . The resulting change in the mass power spectrum depends on how much Ψ deviates from its GR value and the duration of time this deviation lasts. The results for $f(R)$ and DGP models at $z = 0$ are shown in Fig. 3. However a direct probe of Ψ at a given redshift is provided by the distortions of galaxy clustering in redshift space.

Redshift surveys of galaxies provide statistical measurements of clustering over Mpc-Gpc scales. Redshift space distortions in the galaxy power spectrum arise from motions along the line-of-sight – on large scales these are sensitive to the linear growth factor for θ_v , denoted D_v here. It is related to D , the linear density growth factor via the continuity equation as:

$$D_v \propto a\dot{D} = a\beta HD; \quad \beta \equiv d \ln D / d \ln a. \quad (95)$$

Thus redshift space measurements can probe the rate of growth of structure. Different combinations of the information from weak lensing and redshift space galaxy clustering have been used to forecast tests of MG models [195, 196, 197, 182, 198, 190].

The line-of-sight component of peculiar velocities cause the observable redshift-space power spectrum $P_{gg}^{(s)}(k, \mu_k)$ to be ‘squashed’ along the line of sight on large scales (in the linear regime) and to produce pronounced ‘finger-of-God’ features on small scales (in the nonlinear regime) [199, 200]. The directional dependence of $P_{gg}^{(s)}$ is given by $\mu_k \equiv k_{\parallel}/k$, which depends on the angle between a wave vector \mathbf{k} and the line-of-sight direction. Although the picture is more complicated in reality (see [204] for a detailed discussion), it is a good approximation to decompose the redshift space power spectrum in terms of three isotropic power spectra relating the galaxy overdensity $\delta_g = b\delta$ and peculiar velocities \mathbf{v} : the galaxy power spectrum $P_{gg}(k)$, the velocity power spectrum $P_{vv}(k)$ and the cross power spectrum $P_{gv}(k)$ as follows [199]

$$P_{gg}^{(s)}(k, \mu_k) = [P_{gg}(k) + 2\mu_k^2 P_{gv}(k) + \mu_k^4 P_{vv}(k)] F(k^2 \mu_k^2 \sigma_v^2), \quad (96)$$

where the term $F(k^2 \mu_k^2 \sigma_v^2)$ describes non-linear velocity dispersion effects. The angular dependence in the above equation allows us to obtain the component power spectra from $P_{gg}^{(s)}$. $P_{gg}(k)$, the real space power spectrum of galaxies, is the easiest to measure but its interpretation requires knowledge of galaxy bias. The pure velocity power spectrum $P_{vv}(k)$ has the largest error bars, while the cross-spectrum $P_{gv}(k)$ can be estimated more easily.

The combination of $P_{gv}(k)$, which is proportional to bD_v , with the galaxy-shear cross spectrum $C_{g\kappa}$ is a powerful test of gravity [195]. The former probes the growth factor D_v which responds to the Newtonian potential Ψ , while the latter probes the sum of metric potentials. The ratio is independent of galaxy bias. Hence with appropriate redshift binning, these spectra can constrain the ratio of metric potentials. A recent measurement is discussed below.

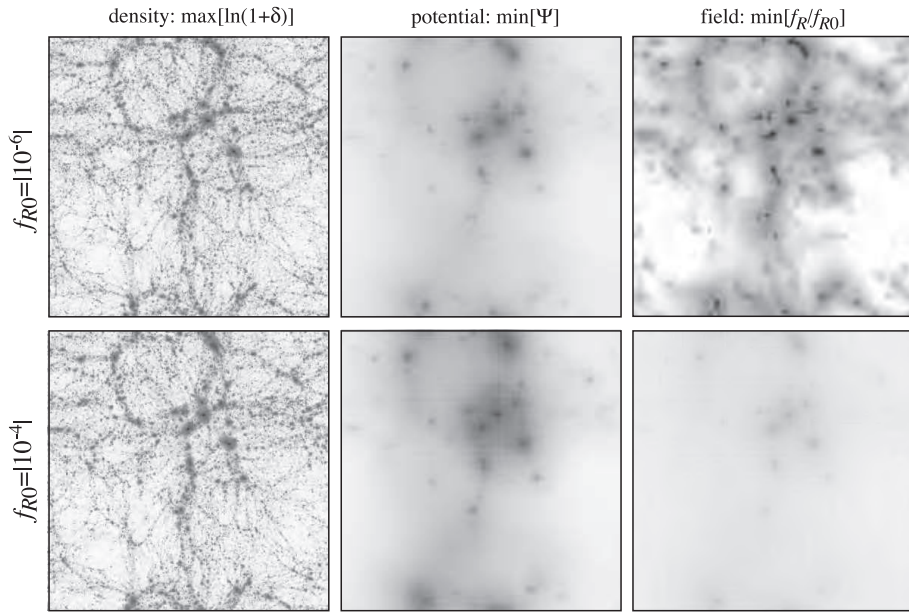


Figure 5: Simulation slices showing the density, potential Ψ and f_R field for two different values of f_{R0} [207]. Along the line of sight through a 2D slice, the maximum of the density and minimum values of Ψ and f_R are shown using a grayscale. In the upper panels the chameleon mechanism is more evident – it suppresses the deviations (from GR) in the potential gradients in massive structures. In the lower panel the chameleon effect is much weaker due to the choice of a larger value of the f_{R0} parameter. These images show qualitatively the coupling between the Newtonian potential and the scalar field in MG gravity theories, and how small scale structure can vary depending on the details of the model.

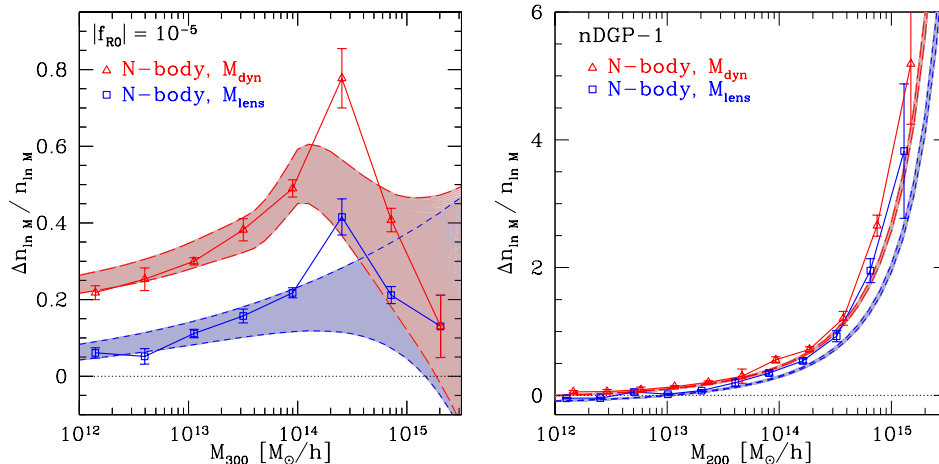


Figure 6: Halo mass functions for $f(R)$ (left panel) and normal branch DGP (right panel) models. The fractional deviation from Λ -CDM are shown using analytical models (shaded regions) and N-body simulations (symbols with error bars) [181]. See text for a discussion of the two definitions of halo mass.

3.2.4. The Nonlinear Regime: Power Spectra and Halo Properties

The nonlinear regime can be demarcated in different ways. While it is standard in cosmology to use the density contrast being close to unity as a rule of thumb, for MG we demarcate it using the breakdown of the linearized equations for the growth of perturbations. Of particular interest is the coupling of the density field to a scalar field such as f_R for $f(R)$ models. A number of papers have recently reported simulations that include such a coupling for both $f(R)$ and DGP gravity [157, 207, 181, 209]. Fig. 5 shows results from such a study by Oyaizu *et al.* [207]. The density, potential and scalar field f_R are shown for two $f(R)$ simulations. It is evident that the qualitative difference in the f_R field leads to a perceptible difference in the potential due to their coupled evolution.

The two primary results from simulations are the nonlinear mass power spectrum and the mass function of galaxy and cluster sized halos [181, 209, 36]. For specific models these predictions allow for comparisons to data. Figures 3 and 6 show the measured power spectra and mass functions from N-body simulations. Simulations and analytical studies [194, 208, 209] also show the transition from a modified gravity regime to GR inside massive halos, due to the Vainshtein or chameleon mechanisms for DGP and $f(R)$ theories respectively. Thus we have the possibility of comparing these MG theories to observations even within and around galaxy and cluster halos. The advantage of such tests is that order unity deviations are expected.

The mass function of cluster sized halos can show strong deviations due to enhanced gravitational forces from the coupling with the scalar field in MG theories. Fig. 6 shows the fractional deviations in the mass function for $f(R)$ and DGP models (similar to the power spectra shown in Fig. 3) [181]. For $f(R)$

models significant departures from GR may occur if scales involved in forming clusters are smaller than the Compton wavelength of the scalar f_R but larger than the scale of chameleon effects that screen halos from the modified forces and drive the theory to GR. Theoretical predictions require careful treatment of spherical collapse in MG theories as screening effects are dependent on halo mass and environment [194].

For cluster masses approaching $10^{15} M_\odot$, the deviations are significant, from enhancements of tens of percent for $f(R)$ to about a factor of 2 for DGP models (note that the DGP model shown in Fig. 6 is the normal branch DGP, which has enhanced forces, similar to $f(R)$ gravity). These departures are driven by the deviation in the linear growth rate on a scale of ~ 10 Mpc, coupled to the exponential dependence of the mass function at the high mass end to this growth rate. In addition, the mass inferred from dynamical measurements differs from the true (lensing) mass for unscreened halos; this amplifies the deviations in the mass function as shown by the upper set of curves in Fig. 6. The resulting observational constraints are summarized next.

3.3. Summary of Current Astrophysical Constraints

Current tests of gravity on astrophysical scales rely on combining probes of the expansion history with the growth of structure. In the literature so far the observations that have been most effectively used for the distance-redshift relation are: CMB, SNIa and BAOs; and for the growth of structure: the CMB power spectrum, ISW cross-correlations, weak lensing shear correlations and the abundance of galaxy clusters (in the nonlinear regime).

Perhaps the tightest formal constraints on gravity have been obtained on galactic scales. [205] and [206] used a combination of strong lensing observations in SDSS galaxies and the dynamics of stars to constrain the ratio of metric potentials. They find the ratio to be consistent with unity, to better than 10%.

Cosmological parameter analyses have been performed by several authors to test gravity in the linear regime of perturbations [210, 140, 211, 212, 213, 214, 215, 216, 217]. In the linear regime (scales $\gtrsim 10$ Mpc) current tests show consistency with GR. For the DGP scenario, [214] have obtained stringent constraints on the self-accelerating branch DGP model. They also find that both normal and self-accelerating branches of DGP require an explicit cosmological constant to be viable. However, generalized braneworld models such as cascading gravity evade these observational constraints.

On scales above 10 Mpc a very recent test of GR [218] comes from comparing galaxy-velocity and galaxy-shear cross-correlations (discussed above in Section 3.2.3) from the SDSS. The $E_G \sim C_{g\kappa}/P_{gv}$ parameter introduced by [195] is a ratio of cross-correlations that is essentially independent of galaxy bias for suitable choices of galaxy redshift distributions. It is estimated to be ~ 0.4 , consistent with its value in GR: $E_G = \Omega_m(z=0)/\beta(z)$, where β is the logarithmic rate of growth parameter introduced above in Eqn. 95. The 20% level measurement of E_G by [218] spans scales of 10-50 Mpc at redshift $z \simeq 0.3$.

The abundance of galaxy clusters from X-ray observations has been used to constrain the growth factor [212] and specific $f(R)$ models [211]. The mass

	f_{sky}	$n_{\text{g}}^{2\text{d}}$	\bar{n}_{g}	$\langle z \rangle$	z_{max}
DES	5000	15	-	0.7	-
Stage-IV	20000	30	-	1.2	-
BOSS	10000	0.05	1.1×10^{-4}	-	0.7
BOSS-II	20000	0.14	1.1×10^{-4}	-	1.1

Table 1: Parameters of imaging and spectroscopic surveys: sky coverage f_{sky} in sq. degs., galaxy surface density $n_{\text{g}}^{2\text{d}}$ per sq. arcmin., the three-dimensional galaxy number density \bar{n}_{g} per Mpc³, the mean redshift $\langle z \rangle$, and the maximum redshift z_{max} .

function can be significantly enhanced at large masses for $f(R)$ and DGP models (see discussion in the previous sub-section). Using information on the mass function requires nonlinear regime model predictions that include chameleon dynamics, hence constraints are specific to particular models. [211] constrain the Compton wavelength to be smaller than ~ 50 Mpc, or equivalently, for the present day field amplitude to be $f_{R0} < 2 \times 10^{-4}$ for their $f(R)$ model. A more recent analysis by [219] combines large-scale structure information with galaxy cluster abundances to find comparable constraints.

Thus current tests of gravity find no indications of departures from GR. The tests in the literature so far are not very stringent in the linear regime, where model-independent constraints on MG parameters are feasible. Tests on smaller scales have been used to test GR by measuring the ratio of dynamical to lensing masses. These tests have constrained the ratio of metric potentials at the tens of percent level. Parameters of specific models of $f(R)$ and DGP gravity have also been constrained. These tests are restricted to narrow ranges in mass/length scale and redshift, and are far less stringent than laboratory or solar system measurements. These limited tests are nevertheless a sign of progress in both theory and observational analysis – a decade ago virtually no tests of GR were available on astrophysical scales. We discuss next the prospects for tests of gravity from upcoming surveys.

3.4. Upcoming Surveys

Planned surveys that will advance low-redshift cosmological measurements include multi-color imaging surveys and spectroscopic surveys of selected galaxies. We consider two planned imaging surveys: the Dark Energy Survey (DES) [220] which is expected to begin data acquisition in 2011, and a generic Stage-IV survey [221, 222, 223, 224] whose example is the LSST survey [222]. A more complete list of two generations of upcoming imaging surveys, and the redshift range covered, is:

- DES, PS1, HSC (2010–). $0 < z \lesssim 1$.
- LSST, JDEM, EUCLID (2016–). $0 < z \lesssim 3$.

The surveys are characterized by sky coverage f_{sky} , surface number density of lensed galaxies $n_{\text{g}}^{2\text{d}}$ and the galaxy redshift distribution. The sky coverage

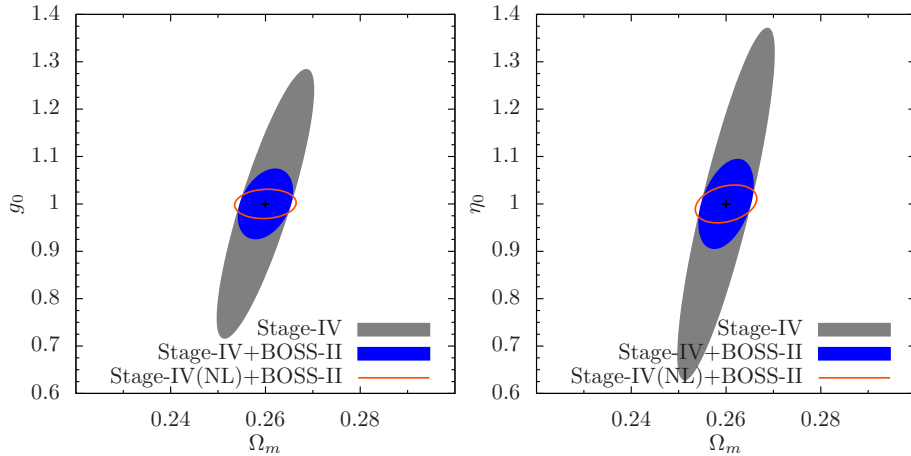


Figure 7: Fisher constraints on modified gravity parameters from planned Stage IV surveys: LSST and BOSS-II [190]. The parameters on the y-axis are $g_0 = G/G_N$ and $\eta_0 = \Phi/\Psi$. The gray contours show the 68% confidence region using just imaging data while the blue contours combine imaging and spectroscopic (lensing and dynamical) information. The inner red contours also use information in the nonlinear, small-scale regime.

for the DES is taken to be 5000 sq. degs. and for the Stage-IV survey 20000 sq. degs. The number density and mean redshifts of the surveys are given in Table 1; see [184] for the detailed redshift distribution used and other parameters.

In order to measure the redshift-space power spectrum $P_{gg}^{(s)}$ we consider spectroscopic surveys of galaxies. While primarily designed to measure the distance-redshift relation and $H(z)$ using the baryon acoustic oscillations in galaxy power spectra, they will provide improved measurements of P_{gg} , P_{gv} , P_{vv} on large scales. Some upcoming spectroscopic galaxy surveys are:

- LAMOST, WiggleZ, HETDEX, BOSS (2010–). $0 < z \lesssim 3$.
- JDEM, EUCLID, BigBOSS (2016–). $0 \lesssim z \lesssim 3$.

As an example of an upcoming survey, we consider the Baryon Oscillation Spectroscopic Survey (BOSS) [225] which will target Luminous Red Galaxies (LRG) up to redshift $z \sim 0.7$ and will cover a quarter of the sky. It will obtain spectra of 1.5×10^6 galaxies. In addition to the BOSS survey we consider a futuristic version (dubbed BOSS-II here; see also the proposed BigBOSS survey [226]) with double the sky coverage compared to BOSS (to keep up with the sky coverage of Stage-IV survey), the same galaxy number density, and extending to redshift $z = 1.1$. Fig. 4 shows the expected accuracy in lensing spectra from the DES and Stage IV surveys. Fig. 7 shows the level of tests of gravity achievable with planned Stage IV surveys [190] using lensing and redshift space power spectra. The constraints on the Gravitational constant and ratio of metric potentials are shown using different combinations of survey data.

There is another kind of redshift survey based on 21 cm radiation from neutral Hydrogen at high redshift. The most ambitious planned survey is the

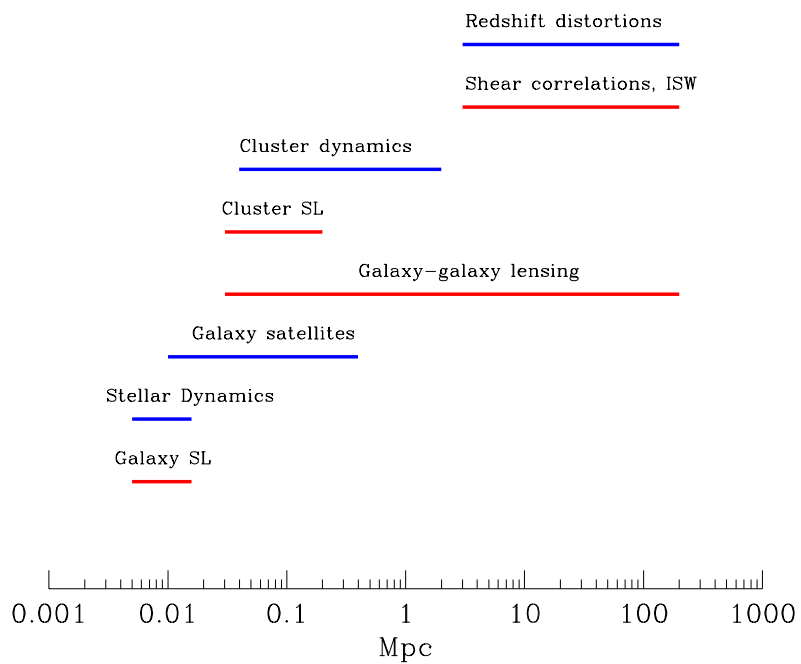


Figure 8: Tests of gravity at different length scales. Red lines shows observations that probe the sum of metric potentials via weak and strong gravitational lensing or the ISW effect. Blue lines show dynamical measurements that rely on the motions of stars or galaxies or other non-relativistic tracers. With upcoming surveys, scales of 100s of Mpc will become accessible, while the accuracy of measurements will improve on all scales.

square kilometer array (SKA) [227](2015–). SKA has the potential to detect ~ 1 billion galaxies over $0 < z \lesssim 1.5$, with a deeper survey extending to $z \sim 5$, through 21cm line emission of neutral hydrogen in galaxies. If successful, it will provide high precision measurements of the distance-redshift relation through BAO's [228], and tests of MG [195] through: weak lensing, velocity measurements through redshift distortions of galaxy clustering, and ISW measurements through CMB-galaxy cross-correlations.

X-ray and SZ cluster surveys (e.g. ACT [229] and SPT [230]) aim to measure the mass function of galaxy clusters out to $z \sim 1$. Cosmological applications will depend on supplementary optical data to get photometric redshifts of the detected clusters. The comparison with lensing masses is essential for the mass calibration, but it will also provide a test of gravity by comparing dynamical and lensing masses.

CMB temperature and polarization maps provide high- z constraints and also measurements of the ISW effect and CMB lensing, which are probes of $\Psi + \Phi$ at lower redshift. In addition to the all-sky PLANCK mission from space, a number of surveys from the ground will provide polarization maps at high angular resolution.

We have indicated the approximate redshift range over which these surveys will provide accurate measurements. Different observables that overlap in redshift and length scale in the range $z \simeq 0.3 - 1$ and at scale $\lambda \simeq 10$ to several 100 Mpc can be compared in the linear and quasilinear regimes of structure formation. It is likely that MG effects are significant on these scales. As emphasized above, on smaller scales of order a Mpc or less, even larger deviations may be expected. Fig. 8 shows the length scales expected to be probed at low redshift by lensing and dynamical probes.

We can expect that theoretical developments will continue to influence observational approaches since no complete formalism exists to provide model independent tests of MG theories on astrophysical scales. It is only for linear fluctuations in the quasi-static, Newtonian regime that the effective Gravitational constant and the ratio of metri potentials are useful effective parameters. New tests in the nonlinear regime will require detailed models and simulations that incorporate the screening mechanisms for specific theories. Combinations of laboratory and solar system tests with astrophysical tests are also promising probes of screening mechanisms. Finally, we note that we have not explored the feasibility of distinguishing modifications of gravity from general dark energy scenarios. Indeed, it is likely that dark energy with small scale clustering that allows for any desired anisotropic stress and pressure will not in practice be distinguishable from the kinds of MG theories we have discussed (e.g. [5, 184]).

4. Discussion

We have reviewed modified gravity theories with interesting cosmological consequences. We focused on higher dimensional approaches and scalar-tensor theories, such as chameleon/ $f(R)$ and symmetron theories. We classified these

models in terms of the screening mechanisms that enable such theories to approach general relativity on small scales. We described general features of the modified Friedman equation in such theories and how they may be distinguished experimentally. The second half of this review discussed experimental test of gravity in light of the new theoretical approaches. We introduced a variety of astrophysical tests that are likely to be valuable in testing gravity theories. Recent progress in modeling the growth of perturbations in MG theories and new observational analyses have led to the first astrophysical tests of gravity. We summarized current constraints, upcoming surveys and prospects for new tests.

5. Acknowledgements

We are indebted to Niayesh Afshordi, Alex Borisov, Claudia de Rham, Gia Dvali, Gregory Gabadadze, Ghazal Geshnizjani, Kurt Hinterbichler, Stefan Hofmann, Wayne Hu, Lam Hui, Kazuya Koyama, Marcos Lima, Alberto Nicolis, Fabian Schmidt, Roman Scoccimarro, Ravi Sheth, Andrew Tolley, Mark Trodden, Amol Upadhye, Jean-Philippe Uzan, Daniel Wesley and Mark Wyman for many enlightening discussions over the years. We thank Pengjie Zhang, Jacek Guzik and Masahiro Takada for collaborative work on which parts of Sec. 3 are based. We are grateful to Fabian Schmidt for comments on the manuscript and for providing us Figs. 3 and 6. This work was partially supported by funds from the University of Pennsylvania and NSERC of Canada (J.K.), and by NSF grant AST-0607667 (B.J.).

References

- [1] C. M. Will, Living Rev. Rel. **9**, 3 (2005) [arXiv:gr-qc/0510072].
- [2] See, *e.g.* E. Komatsu *et al.*, arXiv:1001.4538 [astro-ph.CO]; M. Tegmark *et al.* [SDSS Collaboration], Phys. Rev. D **74**, 123507 (2006) [arXiv:astro-ph/0608632]; A. G. Riess *et al.*, Astrophys. J. **659**, 98 (2007) [arXiv:astro-ph/0611572]; Frieman, J. A., Turner, M. S., & Huterer, D. 2008, Ann. Rev. of Astronoy & Astrophysics, 46, 385; Caldwell, R. R., & Kamionkowski, M. 2009, Ann. Rev. of Nuclear & Particle Science, 59, 397
- [3] S. Weinberg, Rev. Mod. Phys. **61**, 1 (1989).
- [4] A. Silvestri and M. Trodden, Rept. Prog. Phys. **72**, 096901 (2009) [arXiv:0904.0024 [astro-ph.CO]]; Uzan, J.-P. 2009, Space Science Reviews, **148**, 249; Padmanabhan, T. 2008, General Relativity and Gravitation, 40, 529
- [5] M. Kunz and D. Sapone, Phys. Rev. Lett. **98**, 121301 (2007) [arXiv:astro-ph/0612452].
- [6] W. Hu and I. Sawicki, Phys. Rev. D **76**, 104043 (2007) [arXiv:0708.1190 [astro-ph]].

- [7] C. Skordis, Phys. Rev. D **79**, 123527 (2009) [arXiv:0806.1238 [astro-ph]].
- [8] M. Milgrom, Astrophys. J. **270**, 365 (1983).
- [9] J. D. Bekenstein, Phys. Rev. D **70**, 083509 (2004) [Erratum-ibid. D **71**, 069901 (2005)] [arXiv:astro-ph/0403694].
- [10] C. Skordis, Phys. Rev. D **77**, 123502 (2008) [arXiv:0801.1985 [astro-ph]].
- [11] C. Brans and H. Dicke, Phys. Rev. **124**, 925 (1961).
- [12] E. Mach, *The Science of Mechanics: A Critical and Historical Account of Its Development* (1893), translated by T. J. McCormach (Open Court, LaSalle, Illinois, 1960).
- [13] *Mach's Principle: From Newton's Bucket to Quantum Gravity*, edited by J. Barbour and H. Pfister (Birkhauser, Cambridge, 1995).
- [14] C. W. Misner, K. S. Thorne and J. A. Wheeler, *Gravitation. Volume 3.*, Princeton University Library, Princeton, NJ.
- [15] J. Khoury and M. Parikh, arXiv:hep-th/0612117.
- [16] N. Arkani-Hamed, S. Dimopoulos and G. R. Dvali, Phys. Lett. B **429**, 263 (1998) [arXiv:hep-ph/9803315].
- [17] A. Lukas, B. A. Ovrut, K. S. Stelle and D. Waldram, Phys. Rev. D **59**, 086001 (1999) [arXiv:hep-th/9803235].
- [18] L. Randall and R. Sundrum, Phys. Rev. Lett. **83**, 3370 (1999) [arXiv:hep-ph/9905221].
- [19] P. Binetruy, C. Deffayet and D. Langlois, Nucl. Phys. B **565**, 269 (2000) [arXiv:hep-th/9905012].
- [20] P. Brax, C. van de Bruck and A. C. Davis, Rept. Prog. Phys. **67**, 2183 (2004) [arXiv:hep-th/0404011].
- [21] J. Khoury and R. J. Zhang, Phys. Rev. Lett. **89**, 061302 (2002) [arXiv:hep-th/0203274].
- [22] G. R. Dvali, G. Gabadadze and M. Porrati, Phys. Lett. B **485**, 208 (2000) [arXiv:hep-th/0005016].
- [23] G. R. Dvali and G. Gabadadze, Phys. Rev. D **63**, 065007 (2001) [arXiv:hep-th/0008054].
- [24] G. R. Dvali, G. Gabadadze, M. Kolanovic and F. Nitti, Phys. Rev. D **64**, 084004 (2001) [arXiv:hep-ph/0102216].
- [25] For a review, see A. Lue, Phys. Rept. **423**, 1 (2006) [arXiv:astro-ph/0510068].

- [26] N. Arkani-Hamed, H. Georgi and M. D. Schwartz, *Annals Phys.* **305**, 96 (2003).
- [27] M. A. Luty, M. Porrati, and R. Rattazzi, *JHEP* **0309**, 029 (2003) [arXiv:hep-th/0303116].
- [28] A. Nicolis and M. Rattazzi, *JHEP* **0309**, 029 (2003) [arXiv:hep-th/0303116].
- [29] T. Damour, G.W. Gibbons and C. Gundlach, *Phys. Rev. Lett.* **64**, 123 (1990); J.A. Casas, J. Garcia-Bellido and M. Quiros, *Clas. Quant. Grav.* **9**, 1371 (1992); R. Bean, *Phys. Rev. D* **64**, 123516 (2001); D. Comelli, M. Pietroni and A. Riotto, *Phys. Lett. B* **571**, 115 (2003); U. Franca and R. Rosenfeld, *Phys. Rev. D* **69**, 063517 (2004); L. P. Chimento, A. S. Jakubi, D. Pavon and W. Zimdahl, *Phys. Rev. D* **67**, 083513 (2003).
- [30] L. Amendola, *Phys. Rev. D* **62**, 043511 (2000); L. Amendola and D. Tocchini-Valentini, *Phys. Rev. D* **64**, 043509 (2001); L. Amendola, C. Quercellini, D. Tocchini-Valentini and A. Pasqui, *Astrophys. J.* **583**, L53 (2003); L. Amendola and C. Quercellini, *Phys. Rev. D* **68**, 023514 (2003); G. Olivares, F. Atrio-Barandela and D. Pavon, *Phys. Rev. D* **71**, 063523 (2005).
- [31] H. Wei and R. G. Cai, *Phys. Rev. D* **71**, 043504 (2005); D.B. Kaplan, A.E. Nelson and N. Weiner, *Phys. Rev. Lett.* **93**, 091801 (2004); R. D. Peccei, *Phys. Rev. D* **71**, 023527 (2005).
- [32] G.R. Farrar and P.J.E. Peebles, *Astrophys. J.* **604**, 1 (2004); S.S. Gubser and P.J.E. Peebles, *Phys. Rev. D* **70**, 123510 (2004).
- [33] G. Huey and B. D. Wandelt, *Phys. Rev. D* **74**, 023519 (2006) [arXiv:astro-ph/0407196].
- [34] S. M. Carroll, A. De Felice and M. Trodden, *Phys. Rev. D* **71**, 023525 (2005) [arXiv:astro-ph/0408081].
- [35] S. Das, P. S. Corasaniti and J. Khoury, *Phys. Rev. D* **73**, 083509 (2006) [arXiv:astro-ph/0510628].
- [36] M. C. Martino, H. F. Stabenau and R. K. Sheth, *Phys. Rev. D* **79**, 084013 (2009) [arXiv:0812.0200 [astro-ph]].
- [37] M. C. Martino and R. K. Sheth, arXiv:0911.1829 [astro-ph.CO].
- [38] F. Piazza, *New J. Phys.* **11**, 113050 (2009) [arXiv:0907.0765 [hep-th]]; S. Nesseris, F. Piazza and S. Tsujikawa, arXiv:0910.3949 [astro-ph.CO].
- [39] J. Khoury and A. Weltman, *Phys. Rev. Lett.* **93**, 171104 (2004) [arXiv:astro-ph/0309300]; “Chameleon cosmology,” *Phys. Rev. D* **69**, 044026 (2004) [arXiv:astro-ph/0309411].

- [40] S. S. Gubser and J. Khoury, Phys. Rev. D **70**, 104001 (2004) [arXiv:hep-ph/0405231]; A. Upadhye, S. S. Gubser and J. Khoury, Phys. Rev. D **74**, 104024 (2006) [arXiv:hep-ph/0608186].
- [41] P. Brax, C. van de Bruck, A. C. Davis, J. Khoury and A. Weltman, Phys. Rev. D **70**, 123518 (2004) [arXiv:astro-ph/0408415]; AIP Conf. Proc. **736**, 105 (2005) [arXiv:astro-ph/0410103].
- [42] D. F. Mota and D. J. Shaw, Phys. Rev. Lett. **97**, 151102 (2006) [arXiv:hep-ph/0606204]; Phys. Rev. D **75**, 063501 (2007) [arXiv:hep-ph/0608078].
- [43] T. Damour and G. Esposito-Farese, gravitation,” Phys. Rev. Lett. **70**, 2220 (1993).
- [44] S. M. Carroll, V. Duvvuri, M. Trodden and M. S. Turner, Phys. Rev. D **70**, 043528 (2004) [arXiv:astro-ph/0306438].
- [45] S. Capozziello, S. Carloni and A. Troisi, Recent Res. Dev. Astron. Astrophys. **1**, 625 (2003) [arXiv:astro-ph/0303041].
- [46] S. Nojiri and S. D. Odintsov, Phys. Rev. D **68**, 123512 (2003) [arXiv:hep-th/0307288].
- [47] T. P. Sotiriou and V. Faraoni, arXiv:0805.1726 [gr-qc].
- [48] For a review and further references, see A. De Felice and S. Tsujikawa, arXiv:1002.4928 [gr-qc].
- [49] W. Hu and I. Sawicki, Phys. Rev. D **76**, 064004 (2007) [arXiv:0705.1158 [astro-ph]].
- [50] A. A. Starobinsky, JETP Lett. **86**, 157 (2007) [arXiv:0706.2041 [astro-ph]].
- [51] K. Hinterbichler and J. Khoury, arXiv:1001.4525 [hep-th].
- [52] M. Pietroni, Phys. Rev. D **72**, 043535 (2005) [arXiv:astro-ph/0505615]; K. A. Olive and M. Pospelov, Phys. Rev. D **77**, 043524 (2008) [arXiv:0709.3825 [hep-ph]].
- [53] A. I. Vainshtein, Phys. Lett. B **39**, 393 (1972).
- [54] C. Deffayet, G. R. Dvali, G. Gabadadze and A. I. Vainshtein, Phys. Rev. D **65**, 044026 (2002) [arXiv:hep-th/0106001].
- [55] E. Babichev, C. Deffayet and R. Ziour, JHEP **0905**, 098 (2009) [arXiv:0901.0393 [hep-th]]; arXiv:0907.4103 [gr-qc].
- [56] G. R. Dvali, G. Gabadadze, M. Kolanovic and F. Nitti, Phys. Rev. D **65**, 024031 (2002) [arXiv:hep-th/0106058].
- [57] G. Dvali, G. Gabadadze, X. r. Hou and E. Sefusatti, Phys. Rev. D **67**, 044019 (2003) [arXiv:hep-th/0111266].

- [58] C. de Rham, G. Dvali, S. Hofmann, J. Khoury, O. Pujolas, M. Redi and A. J. Tolley, Phys. Rev. Lett. **100**, 251603 (2008) [arXiv:0711.2072 [hep-th]].
- [59] C. de Rham, S. Hofmann, J. Khoury and A. J. Tolley, JCAP **0802**, 011 (2008) [arXiv:0712.2821 [hep-th]].
- [60] G. Dvali, O. Pujolas and M. Redi, Phys. Rev. Lett. **101**, 171303 (2008) [arXiv:0806.3762 [hep-th]].
- [61] C. de Rham, J. Khoury and A. J. Tolley, Phys. Rev. Lett. **103**, 161601 (2009) [arXiv:0907.0473 [hep-th]].
- [62] C. de Rham, J. Khoury and A. J. Tolley, arXiv:1002.1075 [hep-th].
- [63] G. Gabadadze, Phys. Lett. B **681**, 89 (2009) [arXiv:0908.1112 [hep-th]];
- [64] C. de Rham, arXiv:0910.5474 [hep-th].
- [65] N. Agarwal, R. Bean, J. Khoury and M. Trodden, arXiv:0912.3798 [hep-th].
- [66] A. Nicolis, R. Rattazzi and E. Trincherini, Phys. Rev. D **79**, 064036 (2009) [arXiv:0811.2197 [hep-th]].
- [67] C. Deffayet, G. Esposito-Farese and A. Vikman, Phys. Rev. D **79**, 084003 (2009) [arXiv:0901.1314 [hep-th]].
- [68] N. Chow and J. Khoury, Phys. Rev. D **80**, 024037 (2009) [arXiv:0905.1325 [hep-th]].
- [69] E. Babichev, C. Deffayet and R. Ziour, Int. J. Mod. Phys. D **18**, 2147 (2009) [arXiv:0905.2943 [hep-th]].
- [70] F. P. Silva and K. Koyama, Phys. Rev. D **80**, 121301 (2009) [arXiv:0909.4538 [astro-ph.CO]].
- [71] T. Kobayashi, H. Tashiro and D. Suzuki, Phys. Rev. D **81**, 063513 (2010) [arXiv:0912.4641 [astro-ph.CO]].
- [72] T. Kobayashi, arXiv:1003.3281 [astro-ph.CO].
- [73] S. Schlamminger, K. Y. Choi, T. A. Wagner, J. H. Gundlach and E. G. Adelberger, Phys. Rev. Lett. **100**, 041101 (2008) [arXiv:0712.0607 [gr-qc]].
- [74] <http://microscope.onera.fr/> .
- [75] <http://eotvos.dm.unipi.it/nobili>.
- [76] <http://einstein.Stanford.EDU/STEP/>.

- [77] For a review of fifth force searches, see E. Fischbach and C. Talmadge, *The Search for Non-Newtonian Gravity*, (Springer-Verlag, New York, 1999).
- [78] D. J. Kapner, T. S. Cook, E. G. Adelberger, J. H. Gundlach, B. R. Heckel, C. D. Hoyle and H. E. Swanson, Phys. Rev. Lett. **98**, 021101 (2007) [arXiv:hep-ph/0611184].
- [79] E. G. Adelberger, B. R. Heckel, S. A. Hoedl, C. D. Hoyle, D. J. Kapner and A. Upadhye, Phys. Rev. Lett. **98**, 131104 (2007) [arXiv:hep-ph/0611223].
- [80] B. Bertotti, L. Iess and P. Tortora, Nature **425**, 374 (2003).
- [81] S. S. Shapiro, J. L. Davis, D. E. Lebach and J. S. Gregory, Phys. Rev. Lett. **92**, 121101 (2004).
- [82] Shapiro, I.I., in Ashby, N., Bartlett, D.F., and Wyss, W., eds., General Relativity and Gravitation, *Proceedings of the 12th International Conference on General Relativity and Gravitation*, University of Colorado at Boulder, July 28, 1989, 313330, (Cambridge University Press, Cambridge, U.K., New York, U.S.A., 1990).
- [83] K. Nordtvedt, Phys. Rev. **169**, 1014 (1968).
- [84] S. Baessler, B. R. Heckel, E. G. Adelberger, J. H. Gundlach, U. Schmidt and H. E. Swanson, Phys. Rev. Lett. **83**, 3585 (1999).
- [85] P. Brax, C. van de Bruck and A. C. Davis, Phys. Rev. Lett. **99**, 121103 (2007) [arXiv:hep-ph/0703243].
- [86] C. Burrage, A. C. Davis and D. J. Shaw, Phys. Rev. D **79**, 044028 (2009) [arXiv:0809.1763 [astro-ph]].
- [87] P. Brax, C. van de Bruck, A. C. Davis and D. J. Shaw, Phys. Rev. D **78**, 104021 (2008) [arXiv:0806.3415 [astro-ph]].
- [88] I. Zlatev, L. Wang and P.J. Steinhardt, Phys. Rev. Lett. **82**, 896 (1999); P.J. Steinhardt, L. Wang and I. Zlatev, Phys. Rev. D **59**, 12350 (1999).
- [89] R. Bean, E. E. Flanagan and M. Trodden, New J. Phys. **10**, 033006 (2008) [arXiv:0709.1124 [astro-ph]]; Phys. Rev. D **78**, 023009 (2008) [arXiv:0709.1128 [astro-ph]].
- [90] L. Hui, A. Nicolis and C. Stubbs, arXiv:0905.2966 [astro-ph.CO].
- [91] A. S. Chou *et al.* [GammeV Collaboration], Phys. Rev. Lett. **102**, 030402 (2009) [arXiv:0806.2438 [hep-ex]].
- [92] J. H. Steffen and A. Upadhye, Mod. Phys. Lett. A **24**, 2053 (2009) [arXiv:0908.1529 [hep-ex]].
- [93] A. Upadhye, J. H. Steffen and A. Weltman, Phys. Rev. D **81**, 015013 (2010) [arXiv:0911.3906 [hep-ph]].

- [94] M. Ahlers, A. Lindner, A. Ringwald, L. Schrempp and C. Weniger, Phys. Rev. D **77**, 015018 (2008) [arXiv:0710.1555 [hep-ph]].
- [95] H. Gies, D. F. Mota and D. J. Shaw, Phys. Rev. D **77**, 025016 (2008) [arXiv:0710.1556 [hep-ph]].
- [96] C. Burrage, A. C. Davis and D. J. Shaw, Phys. Rev. D **79**, 044028 (2009) [arXiv:0809.1763 [astro-ph]].
- [97] C. Burrage, A. C. Davis and D. J. Shaw, Phys. Rev. Lett. **102**, 201101 (2009) [arXiv:0902.2320 [astro-ph.CO]].
- [98] T. Damour and K. Nordtvedt, Phys. Rev. D **48**, 3436 (1993).
- [99] A. A. Starobinsky, Phys. Lett. B **91**, 99 (1980).
- [100] B. Whitt, Phys. Lett. B **145**, 176 (1984).
- [101] K. i. Maeda, Phys. Rev. D **39**, 3159 (1989).
- [102] L. A. Kofman, V. F. Mukhanov and D. Y. Pogosian, Sov. Phys. JETP **66**, 433 (1987)
- [103] S. M. Carroll, A. De Felice, V. Duvvuri, D. A. Easson, M. Trodden and M. S. Turner, Phys. Rev. D **71**, 063513 (2005) [arXiv:astro-ph/0410031].
- [104] R. P. Woodard, Lect. Notes Phys. **720**, 403 (2007) [arXiv:astro-ph/0601672].
- [105] S. Nojiri and S. D. Odintsov, Phys. Lett. B **631**, 1 (2005) [arXiv:hep-th/0508049].
- [106] A. Upadhye, W. Hu and J. Khoury, to appear.
- [107] A. V. Frolov, Phys. Rev. Lett. **101**, 061103 (2008) [arXiv:0803.2500 [astro-ph]].
- [108] S. A. Appleby and R. A. Battye, JCAP **0805**, 019 (2008) [arXiv:0803.1081 [astro-ph]].
- [109] S. Nojiri and S. D. Odintsov, Phys. Rev. D **78**, 046006 (2008) [arXiv:0804.3519 [hep-th]].
- [110] T. Kobayashi and K. i. Maeda, Phys. Rev. D **78**, 064019 (2008) [arXiv:0807.2503 [astro-ph]].
- [111] A. Upadhye and W. Hu, arXiv:0905.4055 [astro-ph.CO].
- [112] A. Dev, D. Jain, S. Jhingan, S. Nojiri, M. Sami and I. Thongkool, Phys. Rev. D **78**, 083515 (2008) [arXiv:0807.3445 [hep-th]].
- [113] T. Kobayashi and K. i. Maeda, Phys. Rev. D **79**, 024009 (2009) [arXiv:0810.5664 [astro-ph]].

- [114] H. van Dam and M. J. G. Veltman, Nucl. Phys. B **22**, 397 (1970); V. I. Zakharov, JETP Lett. **12**, 312 (1970) [Pisma Zh. Eksp. Teor. Fiz. **12**, 447 (1970)].
- [115] M. Fierz and W. Pauli, Proc. Roy. Soc. Lond. A **173** (1939) 211.
- [116] N. Arkani-Hamed, H. C. Cheng, M. A. Luty and S. Mukohyama, JHEP **0405**, 074 (2004) [arXiv:hep-th/0312099].
- [117] V. A. Rubakov, arXiv:hep-th/0407104.
- [118] S. L. Dubovsky, JHEP **0410**, 076 (2004) [arXiv:hep-th/0409124].
- [119] D. G. Boulware and S. Deser, Phys. Rev. D **6**, 3368 (1972).
- [120] P. Creminelli, A. Nicolis, M. Papucci and E. Trincherini, JHEP **0509**, 003 (2005) [arXiv:hep-th/0505147].
- [121] C. Deffayet and J. W. Rombouts, Phys. Rev. D **72**, 044003 (2005) [arXiv:gr-qc/0505134].
- [122] G. R. Dvali, S. Hofmann, and J. Khoury, Phys. Rev. D **76**, 084006 (2007) [arXiv:hep-th/0703027].
- [123] A. H. Chamseddine and V. Mukhanov, arXiv:1002.3877 [hep-th].
- [124] G. R. Dvali, G. Gabadadze, M. Kolanovic and F. Nitti, Phys. Rev. D **65**, 024031 (2002) [arXiv:hep-th/0106058].
- [125] A. Gruzinov, New Astron. **10**, 311 (2005) [arXiv:astro-ph/0112246].
- [126] M. Porrati, Phys. Lett. B **534**, 209 (2002) [arXiv:hep-th/0203014].
- [127] G. Gabadadze and A. Iglesias, Phys. Rev. D **72**, 084024 (2005) [arXiv:hep-th/0407049].
- [128] T. Tanaka, Phys. Rev. D **69**, 024001 (2004) [arXiv:gr-qc/0305031].
- [129] C. Deffayet, Phys. Lett. B **502**, 199 (2001) [arXiv:hep-th/0010186].
- [130] C. Deffayet, G. R. Dvali and G. Gabadadze, Phys. Rev. D **65**, 044023 (2002) [arXiv:astro-ph/0105068].
- [131] C. Charmousis, R. Gregory, N. Kaloper and A. Padilla, JHEP **0610**, 066 (2006) [arXiv:hep-th/0604086]; K. Koyama, Phys. Rev. D **72**, 123511 (2005) [arXiv:hep-th/0503191].
- [132] N. Kaloper, Phys. Rev. Lett. **94**, 181601 (2005) [Erratum-ibid. **95**, 059901 (2005)] [arXiv:hep-th/0501028]; N. Kaloper, Phys. Rev. D **71**, 086003 (2005) [Erratum-ibid. D **71**, 129905 (2005)] [arXiv:hep-th/0502035].
- [133] D. Gorbunov, K. Koyama and S. Sibiryakov, Phys. Rev. D **73**, 044016 (2006) [arXiv:hep-th/0512097].

- [134] G. Dvali, G. Gabadadze, O. Pujolas and R. Rahman, Phys. Rev. D **75**, 124013 (2007) [arXiv:hep-th/0612016].
- [135] R. Gregory, N. Kaloper, R. C. Myers and A. Padilla, JHEP **0710**, 069 (2007) [arXiv:0707.2666 [hep-th]].
- [136] A. Lue and G. D. Starkman, Phys. Rev. D **70**, 101501 (2004) [arXiv:astro-ph/0408246]; V. Sahni and Y. Shtanov, JCAP **0311**, 014 (2003) [arXiv:astro-ph/0202346].
- [137] G. Gabadadze and A. Iglesias, Phys. Lett. B **639**, 88 (2006) [arXiv:hep-th/0603199].
- [138] A. Adams, N. Arkani-Hamed, S. Dubovsky, A. Nicolis and R. Rattazzi, JHEP **0610**, 014 (2006) [arXiv:hep-th/0602178].
- [139] G. R. Dvali, A. Gruzinov and M. Zaldarriaga, Phys. Rev. D **68**, 024012 (2003) [arXiv:hep-th/0212069].
- [140] N. Afshordi, G. Geshnizjani and J. Khoury, arXiv:0812.2244 [astro-ph].
- [141] J. B. R. Battat, C. W. Stubbs and J. F. Chandler, of gravity,” Phys. Rev. D **78**, 022003 (2008) [arXiv:0805.4466 [gr-qc]].
- [142] E. Adelberger, Private communication; T.W. Murphy, Jr., E.G. Adelberger, J.D. Strasburg and C.W. Stubbs, ‘APOLLO: Multiplexed Lunar Laser Ranging’, at <http://physics.ucsd.edu/~tmurphy/apollo/doc/multiplex.pdf>.
- [143] K. Hinterbichler, A. Nicolis and M. Porrati, arXiv:0905.2359 [hep-th].
- [144] G. Dvali, G. Gabadadze and M. Shifman, Phys. Rev. D **67**, 044020 (2003) [arXiv:hep-th/0202174].
- [145] N. Arkani-Hamed, S. Dimopoulos, G. Dvali and G. Gabadadze, arXiv:hep-th/0209227.
- [146] G. Dvali, New J. Phys. **8**, 326 (2006).
- [147] S. L. Dubovsky and V. A. Rubakov, Phys. Rev. D **67**, 104014 (2003) [arXiv:hep-th/0212222].
- [148] G. Gabadadze and M. Shifman, Phys. Rev. D **69**, 124032 (2004) [arXiv:hep-th/0312289].
- [149] M. Kolanovic, M. Porrati and J. W. Rombouts, Phys. Rev. D **68**, 064018 (2003) [arXiv:hep-th/0304148].
- [150] M. Porrati and J. W. Rombouts, Phys. Rev. D **69**, 122003 (2004) [arXiv:hep-th/0401211].
- [151] R. P. Geroch and J. H. Traschen, Phys. Rev. D **36**, 1017 (1987).

- [152] W. D. Goldberger and M. B. Wise, Phys. Rev. D **65**, 025011 (2002) [arXiv:hep-th/0104170].
- [153] C. de Rham, JHEP **0801**, 060 (2008) [arXiv:0707.0884 [hep-th]].
- [154] C. de Rham, arXiv:0810.0269 [hep-th].
- [155] N. Kaloper and D. Kiley, JHEP **0705**, 045 (2007) [arXiv:hep-th/0703190].
- [156] O. Corradini, K. Koyama and G. Tasinato, Phys. Rev. D **77**, 084006 (2008) [arXiv:0712.0385 [hep-th]]; Phys. Rev. D **78**, 124002 (2008) [arXiv:0803.1850 [hep-th]].
- [157] J. Khoury and M. Wyman, Phys. Rev. D **80**, 064023 (2009) [arXiv:0903.1292 [astro-ph.CO]].
- [158] M. Wyman and J. Khoury, arXiv:1004.2046 [astro-ph.CO].
- [159] M. Minamitsuji, Phys. Lett. B **684**, 92 (2010) [arXiv:0806.2390 [gr-qc]].
- [160] G. W. Gibbons, R. Kallosh and A. D. Linde, JHEP **0101**, 022 (2001) [arXiv:hep-th/0011225].
- [161] J. T. . Giblin, C. de Rham, J. Khoury and A. J. Tolley, in preparation.
- [162] Cedric Deffayet, Kristen Menou. 2007, arXiv:0709.0003
- [163] Iocco, F., Mangano, G., Miele, G., Pisanti, O., & Serpico, P. D. 2009, Phys. Rep., 472, 1
- [164] Zahn, O., & Zaldarriaga, M. 2003, Phys.Rev. D67, 063002
- [165] Galli, S., Melchiorri, A., Smoot, G. F., & Zahn, O. 2009, Phys.Rev.D80, 023508
- [166] M. White, C.S. Kochanek, 2001, ApJ, 560, 539; A. Shirata, T. Shiromizu, N. Yoshida, Y. Suto, Phys. Rev. D71 (2005) 064030; C. Sealfon, L. Verde & R. Jimenez, Phys. Rev. D71 (2005) 083004; H. Stabenau, B. Jain, Phys.Rev. D 74 (2006) 084007; Sereno, M., & Peacock, J. A. 2006, MNRAS, 371, 719; Shirata, A., Suto, Y., Hikage, C., Shiromizu, T., & Yoshida, N. 2007, arXiv:0705.1311; Wang, S., Hui, L., May, M., & Haiman, Z. 2007, Phys.Rev. D, 76, 063503 Koyama, K., Taruya, A., & Hiramatsu, T. 2009, Phys.Rev. D 79, 123512
- [167] C. Skordis, D. F. Mota, P. G. Ferreira, C. Boehm. Phys. Rev.Lett. 96 (2006) 011301 ; C. Skordis, Phys. Rev. D74 (2006) 103513
- [168] S. Dodelson, M. Liguori. 2006, Phys.Rev.Lett. 97 (2006) 231301
- [169] A. Lue, R. Scoccimarro, G. Starkman. Phys.Rev. D69 (2004) 124015

- [170] L. Knox, Y.-S. Song, J.A. Tyson. 2005, astro-ph/0503644; M. Ishak, A. Upadhye, D. N. Spergel. Phys.Rev. D74 (2006) 043513
- [171] K. Koyama, R. Maartens. JCAP 0601 (2006) 016
- [172] T. Koivisto, H. Kurki-Suonio. Class.Quant.Grav. 23 (2006) 2355-2369; T. Koivisto. Phys.Rev. D73 (2006) 083517; B. Li, M.-C. Chu. Phys.Rev. D74 (2006) 104010; Y.-S. Song, W. Hu, I. Sawicki (2006), astro-ph/0610532; B. Li & J. Barrow. 2007, gr-qc/0701111; M. Amarguioui O. Elgaroy David F. Mota T. Multamaki, 2007, A & A, 454, 707
- [173] P. Zhang. Phys.Rev. D73 (2006) 123504
- [174] R. Bean, D. Bernat, L. Pogosian, A. Silvestri, M. Trodden. Phys.Rev. D75 (2007) 064020
- [175] E. Linder. Phys.Rev. D72 (2005) 043529; D. Huterer, E.Linder. 2006, astro-ph/0608681
- [176] J.-P. Uzan. 2006, arXiv:astro-ph/0605313.
- [177] R. Caldwell, C. Cooray, A. Melchiorri, 2007, astro-ph/0703375
- [178] L. Amendola, M. Kunz, D. Sapone, 2007, arXiv:0704.2421
- [179] Bertschinger, E. 2006, ApJ, 648, 797
- [180] C.-P. Ma, E. Bertschinger. Astrophys.J. 455 (1995) 7-25
- [181] Oyaizu, H., Lima, M., & Hu, W. 2008, Phys. Rev. D **78**, 123524
F. Schmidt, Phys. Rev. D **80**, 043001 (2009) [arXiv:0905.0858 [astro-ph.CO]]; Phys. Rev. D **80**, 123003 (2009) [arXiv:0910.0235 [astro-ph.CO]]; Schmidt, F., Hu, W., & Lima, M. 2010, Phys. Rev. D, **81**, 063005 .
- [182] G.-B. Zhao, L. Pogosian, A. Silvestri, and J. Zylberberg, Phys.Rev. D**79** 003513 (2009)
- [183] Amin, M. A., Wagoner, R. V., & Blandford, R. D. 2008, MNRAS, 390, 131.
- [184] Jain, B., & Zhang, P. 2008, Phys. Rev. D, 78, 063503.
- [185] R.K. Sachs and A.M. Wolfe, 1967, ApJ, 147, 73
- [186] e.g. A. Cabre, E. Gaztanaga, M. Manera, P. Fosalba, F. Castander, MNRAS 372 (2006) L23-L27; D. Pietrobon, A. Balbi, D. Marinucci. Phys.Rev. D74 (2006) 043524; T. Giannantonio et al. Phys.Rev. D74 (2006) 063520; Ho, S., Hirata, C., Padmanabhan, N., Seljak, U., & Bahcall, N. 2008, Phys.Rev. D 78, 043519
- [187] Carroll, S. 2004, "Spacetime and Geometry", Addison-Wesley

- [188] D. N. Limber, ApJ **117**, 134 (1953)
- [189] W. Hu, ApJL **522**, L21 (1999)
- [190] Guzik J., Jain B., Takada M. ArXiv e-prints, arXiv:0906.2221-(2009)
- [191] Hoekstra, H., & Jain, B. 2008, Ann. Rev. of Nuclear & Particle Science, 58, 99
- [192] J. P. Bruneton, and G. Esposito-Farese, Phys.Rev. D**76**, 124012 (2007)
- [193] Heavens, A. F., Kitching, T. D., & Verde, L. 2007, MNRAS, **380**, 1029
- [194] Schmidt, F. 2010, arXiv:1003.0409
- [195] P. Zhang, M. Liguori, R. Bean, and S. Dodelson, Phys.Rev.Lett. **99**, 141302 (2007)
- [196] V. Acquaviva, A. Hajian, D. N. Spergel, and S. Das, Phys.Rev. D**78**, 043514 (2008)
- [197] Y.-S. Song and O. Doré, JCAP **3**, 25 (2009)
- [198] G.-B. Zhao, L. Pogosian, A. Silvestri, and J. Zylberberg, arXiv:0905.1326
- [199] N. Kaiser, MNRAS **227**, 1 (1987)
- [200] A. J. S. Hamilton, in *The Evolving Universe*, Astrophysics and Space Science Library Series **231**, 185 (1998)
- [201] M. Tegmark et al. (SDSS), ApJ **606**, 702 (2004)
- [202] F. Bernardeau, S. Colombi, E. Gaztañaga, and R. Scoccimarro, Physics Reports **367**, 1 (2002)
- [203] M. Tegmark and A. J. S. Hamilton, MNRAS **335**, 887 (2002)
- [204] R. Scoccimarro, Phys.Rev. D**70**, 083007 (2004)
- [205] Bolton, A. S., Rappaport, S., & Burles, S. 2006, Phys.Rev. D, 74, 061501
- [206] Schwab, J., Bolton, A. S., & Rappaport, S. A. 2010, ApJ, 708, 750
- [207] Oyaizu H., Lima M., Hu W. Physical Review D, 78:123524-(2008)
- [208] Smith, T. L. 2009, arXiv:0907.4829
- [209] R. Scoccimarro, Phys. Rev. D **80**, 104006 (2009) [arXiv:0906.4545 [astro-ph.CO]]; K. C. Chan and R. Scoccimarro, Phys. Rev. D **80**, 104005 (2009) [arXiv:0906.4548 [astro-ph.CO]].
- [210] Song, Y.-S., Peiris, H., & Hu, W. 2007, PRD, 76, 063517
- [211] Schmidt, F., Vikhlinin, A., & Hu, W. 2009, Phys.Rev. D **80**, 083505

- [212] Rapetti, D., Allen, S. W., Mantz, A., & Ebeling, H. 2009, arXiv:0911.1787
- [213] Giannantonio, T., Martinelli, M., Silvestri, A., & Melchiorri, A. 2009, arXiv:0909.2045
- [214] Lombriser, L., Hu, W., Fang, W., & Seljak, U. 2009, Phys. Rev. D, 80, 063536
- [215] Bean, R., & Tangmatitham, M. 2010, arXiv:1002.4197
- [216] Daniel, S. F., Linder, E. V., Smith, T. L., Caldwell, R. R., Cooray, A., Leauthaud, A., & Lombriser, L. 2010, arXiv:1002.1962
- [217] Zhao, G.-B., Giannantonio, T., Pogosian, L., Silvestri, A., Bacon, D. J., Koyama, K., Nichol, R. C., & Song, Y.-S. 2010, arXiv:1003.0001
- [218] Reyes, R., Mandelbaum, R., Seljak, U., Baldauf, T., Gunn, J. E., Lombriser, L., & Smith, R. E. 2010, Nature, 464, 256
- [219] Lombriser, L., Slosar, A., Seljak, U., & Hu, W. 2010, arXiv:1003.3009
- [220] <http://www.darkenergysurvey.org>
- [221] A. Albrecht et al. (DETF), astro-ph/0609591
- [222] <http://www.lsst.org>
- [223] <http://jdem.gsfc.nasa.gov>
- [224] <http://sci.esa.int/euclid/>
- [225] <http://cosmology.lbl.gov/BOSS>
- [226] <http://bigboss.lbl.gov/>
- [227] <http://www.skatelescope.org/>
- [228] Abdalla, F. B., & Rawlings, S. 2005, MNRAS, 360, 27.
- [229] <http://www.phy.princeton.edu/act/about.html>
- [230] <http://pole.uchicago.edu/>